BRL

TECHNICAL REPORT BRL-TR-2595

LAUNCH DYNAMICS OF APFSDS AMMUNITION

Peter Plostins

October 1984

US ARMY BALLISTIC RESEARCH LABORATORY
ABERDEEN PROVING GROUND, MARYLAND

Destroy this report when it is no longer needed.
Do not return it to the originator.

Additional copies of this report may be obtained from the National Technical Information Service, U. S. Department of Commerce, Springfield, Virginia 22161.

The findings in this report are not to be construed as an official Department of the Army position, unless so designated by other authorized documents.

The use of trade names or manufacturers' names in this report does not constitute indorsement of any commercial product.

UNCLASSIFIED

SECURITY CLASSIFICATION OF THIS PAGE (When Data Entered)

REPORT DOCUMENTATION PAGE		READ INSTRUCTIONS BEFORE COMPLETING FORM
1. REPORT NUMBER TECHNICAL REPORT BRL-TR-2595	2. GOVT ACCESSION NO. ADA147374	3. RECIPIENT'S CATALOG NUMBER
4. TITLE (and Subtitle) LAUNCH DYNAMICS OF APFSDS AMMUNITION		5. TYPE OF REPORT & PERIOD COVERED Final 6. PERFORMING ORG. REPORT NUMBER
7. AUTHOR(s) Peter Plostins		8. CONTRACT OR GRANT NUMBER(s)
9. PERFORMING ORGANIZATION NAME AND ADDRESS U.S. Army Ballistic Research Laboratory ATTN: AMXBR-LFD Aberdeen Proving Ground, Maryland 21005		10. PROGRAM ELEMENT, PROJECT, TASK AREA & WORK UNIT NUMBERS RDT&E 1L162618AH80
11. CONTROLLING OFFICE NAME AND ADDRESS US Army Ballistic Research Laboratory ATTN: AMXBR-OD-ST Aberdeen Proving Ground, MD 21005-5066		12. REPORT DATE October 1984 13. NUMBER OF PAGES 53
14. MONITORING AGENCY NAME & ADDRESS(if different from Controlling Office)		15. SECURITY CLASS. (of this report) Unclassified 15a. DECLASSIFICATION/DOWNGRADING SCHEDULE

16. DISTRIBUTION STATEMENT (of this Report)

Approved for public release, distribution unlimited.

17. DISTRIBUTION STATEMENT (of the abstract entered in Block 20, if different from Report)

18. SUPPLEMENTARY NOTES

19. KEY WORDS (Continue on reverse side if necessary and identify by block number)

Launch Dynamics
Sabot Discard
Discard Disturbances
APFSDS Ammunition

20. ABSTRACT (Continue on reverse side if necessary and identify by block number)

An experimental program to determine the magnitude and nature of the launch perturbations to the projectile angular motion during sabot discard is discussed. The data analysis isolates the sources and quantifies the severity of the launch perturbations. An explanation of how the discard dynamics may be related to the inbore motion of the round is presented.

The results show that the discard disturbances cause a net increase of 41% in the level of first maximum yaw. For the different configurations tested

DD FORM 1 JAN 73 1473 EDITION OF 1 NOV 65 IS OBSOLETE

UNCLASSIFIED

SECURITY CLASSIFICATION OF THIS PAGE (When Data Entered)

20. ABSTRACT (Continued)

changes in the inbore contribution to first maximum yaw indicate that the structural design of the front boreriding system is critical to the inbore behavior. A correlation is given between the angular rate to angle ratio at the muzzle and the severity of the discard interactions. Based on the correlation an alternate launch philosophy is necessary for APFSDS ammunition to assure on target accuracy.

TABLE OF CONTENTS

		Page
	LIST OF ILLUSTRATIONS	5
I.	INTRODUCTION	7
II.	TEST PRELIMINARIES AND TEST MATRIX	9
III.	DATA ACQUISITION AND INSTRUMENTATION	10
IV.	DATA REDUCTION AND TEST RESULTS	11
	A. First Magnitude of Yaw Effects	13
	B. Mechanical Separation	13
V.	ANALYSIS	14
VI.	SUMMARY	19
VII.	CONCLUSIONS	20
	ACKNOWLEDGMENTS	44
	REFERENCES	45
	LIST OF SYMBOLS	47
	DISTRIBUTION LIST	49

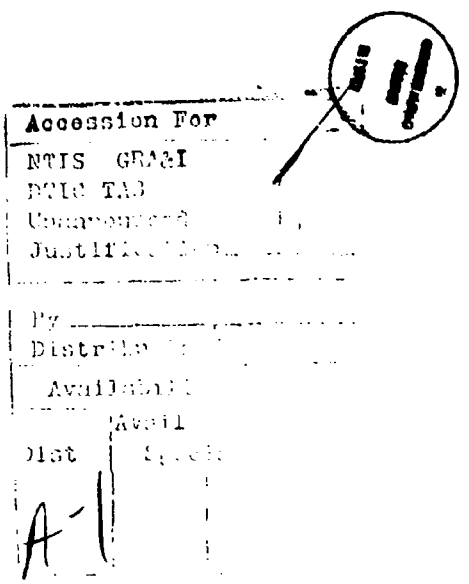

LIST OF ILLUSTRATIONS

Figure		Page
1	Test Round and Sabots	22
2	Bent Sabot	22
3	Schematic of the Test Range	23
4	Orthogonal X-Ray Apparatus	24
5	Discard Sequence X-Ray Data	25
	a. Muzzle Exit	25
	b. Mechanical Interaction	25
	c. Sabot Separation	26
	d. Aerodynamic Interference	26
	e. Initiation of Penetrator Free Flight	27
	f. Free Flight	27
6	Penetrator Coordinate System	28
7	Angular X-Ray Data Standard Penetrator	29
	a. Magnitude of Yaw	29
	b. Angle of Attack	29
	c. Angle of Sideslip	30
8	Transonic Range Yaw Fit	30
9	Comparison of X-Ray Data to Yaw Prediction	31
	a. Proof Slug	31
	b. Standard Penetrator	31
10	Increase in First Max Yaw Due to Discard Disturbances	32
	a. Definition of First Max Yaw	32
	b. First Max Yaw Summary	32
11	Composition of First Max Yaw	33
	a. Composition of First Max Yaw	33
	b. Summary of the Composition of First Max Yaw	33

LIST OF ILLUSTRATIONS (continued)

Figure		Page
12	Normalized Yaw vs. Downrange Distance Similarity Coordinates	34
	a. Standard Penetrator Round Numbers 1-7.....	34
	b. Standard Penetrator Round Numbers 8-14.....	34
	c. Sub-Bore Span Fins Round Numbers 16-20.....	35
	d. Vented Sabot Package Round Numbers 21-25.....	35
13	Inbore Representation of Sabot-Penetrator System.....	36
14	Correlation of the Discard Disturbance to the Initial Conditions..	37
	a. Definition of the Discard Disturbance - Δn.....	37
	b. Discard Disturbance vs. Initial Angular Rate to Angle Ratio...	37
15	Comparison of the Present Data to Previous Data.....	38
16	Comparison of the Discard Disturbance Correlations.....	38
17	Discard Disturbances in the Alpha and Beta Planes.....	39
	a. Proof Slug.....	39
	b. Standard Penetrator.....	39
	c. Penetrator-Vented Sabot Package.....	40
	d. Standard Penetrator.....	40
	e. Standard Penetrator.....	41
	f. Penetrator with Sub-Bore Span Fins.....	41
18	Angle of Attack vs. Angle of Sideslip.....	42
	a. Standard Penetrator.....	42
	b. Standard Penetrator.....	42
19	Alpha and Beta Plane Discard Disturbance Correlation to the Initial Conditions.....	43
	a. Plane of Angle of Attack.....	43
	b. Plane of Sideslip.....	43

I. INTRODUCTION

Modern cannon-fired, anti-armor ammunition consist of high density, subcaliber, fin-stabilized projectiles which are launched within sabots. Figure (1) shows such a kinetic energy device with examples of sabots. The Armor Piercing, Fin-Stabilized, Discarding Sabot (APFSDS) munition weighs less than a full-bore projectile and can be launched at higher velocities. The penetration capability of the long, low-drag, fin-stabilized rod is directly related to its striking velocity. The discarding sabot is used to provide support for the rod and obturation of the gun gases during launch. As the munition exits the gun, interactions between gun, sabot, and projectile occur. These interactions set the initial conditions for subsequent dynamic and aerodynamic performance of the penetrator[1] as well as for the dispersion characteristics.[2]

Saboted rounds may experience additional interactions during the sabot discard process. The higher drag sabot components are removed from the flight vehicle in a manner which can produce a variety of disturbances.[3-8] As the

---

1. *W. H. Drysdale, "Design of Kinetic Energy Projectiles for Structural Integrity," U. S. Army Ballistic Research Laboratory, Aberdeen Proving Ground, Maryland, BRL Report ARBRL-TR-02365, September 1981 (AD A105502).*

2. *C. H. Murphy, "Free Flight Motion of Symmetric Missile," U. S. Army Ballistic Research Laboratory, Aberdeen Proving Ground, Maryland, BRL Technical Report 1216, July 1963 (AD 442757).*

3. *E. M. Schmidt, "Disturbance to the Launch of Fin-Stabilized Projectiles," Journal of Spacecraft and Rockets, Vol. 19, No. 1, January-February 1982, p. 30.*

4. *E. M. Schmidt and D. D. Shear, "Aerodynamic Interference During Sabot Discard," U. S. Army Ballistic Research Laboratory, Aberdeen Proving Ground, Maryland, BRL Report 2019, September 1977 (AD 050308). Also Journal of Spacecraft and Rockets, Vol. 15, No. 3, May-June 1978, pp. 162-167.*

5. *E. M. Schmidt and D. D. Shear, "Launch Dynamics of a Single Flechette Round," U. S. Army Ballistic Research Laboratory, Aberdeen Proving Ground, Maryland, BRL Report 1810, August 1975 (AD B006781).*

6. *W. D. Glaus, "Estimation of the Forces on a Single Flechette Resulting from a Shock Wave," Midwest Research Institute, Kansas City, Missouri, Final Report 19 June 1970 - 18 March 1971, May 1971 (AD 724178).*

7. *G. Glota, "Investigation of the Stability of the Flow During the Sabot Discard Process," Sixth International Symposium on Ballistics, Orlando, Florida, 27-29 October 1981.*

8. *P. Crimi and D. Siegelman, "Analysis of Mechanical and Gasdynamic Loadings During Sabot Discard from Gun-Launched Projectiles," U. S. Army Ballistic Research Laboratory, Aberdeen Proving Ground, Maryland, BRL Contract Report 341, June 1977 (AD B020019).*

shot emerges from the gun tube, elastic decompression together with the residual inertia of the sabot components start the discard sequence. Dynamic and aerodynamic loads on the sabot parts force them away from the projectile. Any existing geometric asymmetries in sabot components may cause a momentum exchange between the components and the long rod flight vehicle. As separation proceeds, air flow is established between the sabot parts and the projectile;[7] strong aerodynamic interactions occur and become the dominant source of the discard disturbance. Schmidt[3] has observed that the two dominant discard mechanisms are mechanical contact and aerodynamic interaction. Flow field asymmetries have their primary effect on the projectile fins where skewed shock patterns have been observed by Schmidt and Shear.[4] Wind tunnel data for the pressures on symmetric and asymmetric sabot configurations have been obtained by Schmidt and Plostins.[9,10] Mechanical impacts have been observed by Schmidt et. al.[11] for the case of a spin-stabilized penetrator.

The initial dynamics of the penetrator are established during the launch process; therefore, it is important to size and determine the contributions of various phases of the launch cycle to the flight dynamics of the projectile. This report presents the results of one part of a test program on an APFSDS projectile. The program was to study launch problems and propose methods for the mitigation of launch disturbances. Only the sabot discard and discard effects on other portions of the launch cycle are discussed here. An analysis of the perturbations to the projectile angular motion due to inbore, mechanical, and aerodynamic interactions during launch are presented.

The comprehensive test program was a joint effort by the Interior Ballistics Division (IBD) and the Launch and Flight Division (LFD) of the Ballistic Research Laboratory (BRL). IBD was responsible for determining the inbore behavior of the rounds using doppler radar.[12] The LFD was responsible for measurement of the aerodynamic performance of the penetrator and the sabot

---

9. *E. M. Schmidt, "Wind Tunnel Measurements of Sabot Discard Aerodynamics," U. S. Army Ballistic Research Laboratory, Aberdeen Proving Ground, Maryland, BRL Technical Report ARBRL-TR-02246, July 1980 (AD 088900).*

10. *E. M. Schmidt and P. Plostins, "Aerodynamics of Asymmetric Sabot Discard," U. S. Army Ballistic Research Laboratory, Aberdeen Proving Ground, Maryland, BRL Report ARBRL-MR-03281, June 1983 (AD 130011).*

11. *E. M. Schmidt, B. P. Burns, and G. Samos, "Replica Modeling of the Launch and Flight Dynamics of Projectiles," U. S. Army Ballistic Research Laboratory, Aberdeen Proving Ground, Maryland, BRL Technical Report ARBRL-TR-02104, September 1978 (AD A063521).*

12. *J. N. Walbert, "Analysis of the In Bore Motion of Several Types of Projectiles," U. S. Army Ballistic Research Laboratory, Aberdeen Proving Ground, Maryland, BRL Memorandum Report ARBRL-MR-03293, July 1983 (AD B076398L).*

discard process. The test program was conducted at the Transonic Range facility[13,14] of the BRL.

II. TEST PRELIMINARIES AND TEST MATRIX

It was desired to test a projectile with improved flight and terminal performance. The design improvements consisted of a lengthened penetrator body with increased sabot load-bearing surface and a reduction of fin span to decrease aerodynamic drag. The standard penetrator, Figure (1), is equipped with bore-riding fins to provide inbore stability. The drag coefficient of the improved model was less than the standard projectile but at the expense of inbore stability. As a result of these changes, the dispersion of the improved projectile was greater than that of the standard projectile.

The long sabot also showed signs of permanent deformation, Figure (2). The aerodynamic liftoff characteristics of the sabots tested caused sabot tail deformation. Large initial sabot petal rotation produced significant loads at the sabot tails which were the pivot points of the rotation. It was necessary to change the initial lift and moment coefficients of the sabot components in an attempt to alleviate the effects of this mechanical interaction. The sabot lift was reduced on five test rounds by removing lift area through a venting procedure. Figure (1) shows a vented sabot petal. A first estimate of the effect of venting the sabot was computed using the AVCO Sabot Discard Code.[8,15-17] Both vented and non-vented cases were run. The code consists of a dynamics package with a six-degree-of-freedom model for the sabot petals and a three-degree-of-freedom angular model for the penetrator, as well as a sabot-penetrator interaction package and an aerodynamic interaction package. The aerodynamic package is based on shock expansion theory.

---

13. *W. F. Braun, "Fiducial Systems for Free Flight Spark Ranges," U. S. Army Ballistic Research Laboratory, Aberdeen Proving Ground, Maryland, BRL Memorandum Report BRLMR 2009, September 1969 (AD 860693).*

14. *C. H. Murphy, "Data Reduction for Free Flight Spark Ranges," U. S. Army Ballistic Research Laboratory, Aberdeen Proving Ground, Maryland, BRL Report BRLR 900, February 1954 (AD 35833).*

15. *P. Crimi and D. Siegelman, "Projectile/Sabot Discard Aerodynamics," U. S. Army Ballistic Research Laboratory, Aberdeen Proving Ground, Maryland, BRL Contract Report ARBRL-CR-410, December 1979 (AD 080538).*

16. *D. Siegleman and J. Wang, "Sabot Design Optimization," U. S. Army Ballistic Research Laboratory, Aberdeen Proving Ground, Maryland, BRL Contract Report ARBRL-CR-450, March 1981 (AD 100264).*

17. *D. Siegelman, J. Wang, and P. Crimi, "Computation of Sabot Discard," U. S. Army Ballistic Research Laboratory, Aberdeen Proving Ground, Maryland, BRL Contract Report ARBRL-CR-505, February 1983 (AD B0715192).*

The measure of the severity of discard interaction is the integrated angular impulse experienced by the penetrator during the discard sequence.

$$\text{Total Angular Discard Impulse} = I = Im + Ia \tag{1}$$

$$Im = \int_0^t Mm\, dt \qquad Ia = \int_0^t Ma\, dt \tag{2}$$

where Ma is the total moment due to aerodynamic loads and Mm is the total moment due to mechanical loads. The results of running the code showed that a 50% vent (based on area) in the sabot cup would reduce the mechanical impulse, Im, by 57%. The mechanical interaction model in the code[8] provides a linear variation of impulse with vent area. The limit to the size of the vent hole is, however, set by considerations of mechanical strength of the sabot petal. Thus, the sabots of five standard rounds were modified to provide vent holes which reduced the front cup lift area by 21%. The introduction of vent holes to the sabot cups had the unfavorable consequence of increasing the time during which discard interactions occur. Even though the sabot tail mechanical interaction force might be reduced through venting, the increased discard time could result in greater total interaction impulses. It was decided to test the five rounds with vented sabots to determine the effect of lift reduction on discard behavior.

A total of twenty-seven rounds were tested. Two were proof slugs, fired to calibrate the test equipment. Proof slugs mimic the sabot-penetrator shot inbore. They are monolithic, without moving parts. Fifteen standard rounds with borespan fins and non-vented sabots were fired to provide a baseline for comparison with the experimental models. Two experimental groups of five rounds each were fired to determine the effects of sub-borespan fins and the effects of vented sabot petals. The first five rounds used the lengthened penetrator with sub-borespan fins and the standard sabot. The second five rounds used the lengthened penetrator with borespan fins and the vented sabot. Twelve of the above penetrators were modified by establishing a radar-reflective flat surface at the nose for doppler radar measurements. The proof slugs have full frontal flat surfaces.

One caliber is defined as the diameter of the body of the penetrator. The standard test projectile had 3.91 caliber borespan fins and a length-to-diameter ratio of 23. The sub-borespan fins had the same surface area as the borespan fins but were 3.31 calibers in diameter. The ratio of moments of inertia Ix/Iy was 4.46×10^{-03} and the transverse radius of gyration was 5.91 calibers and the axial radius of gyration was .395 calibers. The penetrator with sub-borespan fins had practically the same inertial properties.

III. DATA ACQUISITION AND INSTRUMENTATION

A schematic of the experimental test setup is shown in Figure (3). The discard sequence data were obtained from six orthogonal x-ray stations which covered the first 460.5 calibers of penetrator travel. Free flight data of the penetrator motion were collected in the Transonic Range facility. The

instrumented Transonic Range consists of an orthogonal array of 25 spark stations covering a 207 metre length of the flight path. The first station, number 1-1, was considered the zero point of the test. The muzzle of the gun was located 2031.4 calibers uprange from station 1-1. The x-ray apparatus, Figure (4), was calibrated with a fiducial cable strung through the six stations along the line of fire. Three fiducial beads are located at the centerline intersection of the x-ray heads as shown in Figure (5a). The center bead was surveyed into the Transonic Range coordinate system. The outer two beads provide a measure of image magnification on the x-ray plate. In the range coordinate system, the z axis is along the line of fire, the x axis is positive to the left looking downrange, and the y axis is in the recoil plane of the gun to form an orthogonal triad. The locations of the six center beads along the line of fire were surveyed:

Station Number	Location	
1	z = -2020.5 cal	(3a)
2	z = -1924.5 cal	(3b)
3	z = -1826.4 cal	(3c)
4	z = -1721.0 cal	(3d)
5	z = -1639.8 cal	(3e)
6	z = -1560.0 cal	(3f)

A low level x-ray photograph of the cable was taken before each firing. The cable was then removed from the line of fire and a second exposure of the film recorded the penetrator and sabot motion during the test. Thus, the double exposure contains a record of the fiducial cable, the penetrator, and the sabot. Figure (5) is an example of the type of x-ray data obtained.

The x-ray heads used for the test were two 180 KV units at stations one and two and eight 150 KV units for stations three thru six of the x-ray setup. Digital counters, accurate to 0.1 microsecond, were used to obtain time intervals between stations. A photodiode which detected the muzzle flash was used to trigger the x-ray delay units and digital counters.

IV. DATA REDUCTION AND TEST RESULTS

The data obtained from the tests were orthogonal x-ray photographs and time measurements. The x-ray photographs show the fiducial cable, the fiducial beads, and the model and sabot components. Since x-rays are conical sources, objects close to the x-ray heads appear larger on the photographs than objects farther from the heads. For these tests, however, only the penetrator performance was measured and the deviation of the penetrator trajectory from the line of fire was sufficiently small to allow magnification errors to be ignored. A detailed discussion of errors in range x-ray photography is given in Reference 5, Appendix A.

The orthogonal x-ray photographs are measured to provide the location of the center of gravity of the model as a function of downrange position and the angular orientation of the model with respect to the velocity vector. The angle of attack, α, and the angle of sideslip, β, are thus determined. These

angles are depicted in Figure (6). The angle, δ, is defined as the magnitude of the local angle of attack, or the angle between the penetrator axis of symmetry and the velocity vector. For small angles, δ is given by

$$\delta \approx (\alpha^2 + \beta^2)^{1/2}. \tag{4}$$

Figures (7a-c) show typical angular behavior for a standard penetrator. For a penetrator in free flight, the dominant applied torque is the aerodynamic static moment. During sabot discard, an additional applied torque due to the discard mechanism must be considered. Most discard loads are applied at or near the penetrator fins. Hence, a small force may be magnified by a long moment arm to produce a substantial torque. It is hoped that the analysis of the photgraphic data taken in these tests will produce a measure of the effects of the discard torque loadings.

In addition to the orthogonal x-ray data taken during the tests, free flight range data relevant to the aerodynamic behavior of the rounds were obtained in the Transonic Range. The important aerodynamic coefficients measured were C_D the drag coefficient, $C\ell_\alpha$, the lift curve slope, and Cm_α, the static moment coefficient. The results of the standard range reduction procedure[2] also produce a history of the yawing motion within the range. A typical yawing history based on a fit of the reduced range data for a standard penetrator is shown in Figure (8). The fitted curve between the muzzle and station 1-1 was the result of extrapolation. From the fitted data, values of the first maximum yaw, δ_{max}, the initial angular rate, δ_0', and the initial yaw, δ_0, can be obtained. These values are a direct measure of the total launch disturbance experienced by the penetrator. The customary assumptions are that the launch disturbance occurs at the muzzle of the gun and is entirely due to inbore effects. For the case of saboted projectiles, additional disturbances must be accounted for in the transition region between muzzle and free flight.

The initial angular rates at the muzzle are computed by taking first differences of the data at the first two x-ray stations. To obtain the yawing motion from the first differences, certain simplifying assumptions are made: (1) at the muzzle the round is not rolling (smooth bore gun); (2) damping is negligible (less than one cycle of yaw is observed); and (3) gravity need not be considered (short segment of trajectory). The angular motion, then, is

$$\tilde{\xi} = (\tilde{\xi}_0' / \phi') \sin(\phi' S) + \tilde{\xi}_0 \cos(\phi' S) \tag{5}$$

where, $\tilde{\xi}$ is the complex angle of yaw, $\tilde{\xi}_0$ is the complex initial angle of yaw, ξ_0' is the complex initial angular rate, S is the distance along the trajectory, and ϕ' is the yaw frequency. Prime, $'$, denotes differentiation with respect to distance. The magnitude of yaw, δ, is identically the magnitude of the complex angle of yaw, $\tilde{\xi}$. Thus, the yaw frequency is related to the static moment coefficient by:

$$\phi' = [(\rho Ad^3/2I_y)\ Cm_\alpha]^{1/2}. \quad (6)$$

Typically, the yaw frequency of the test penetrators considered in the test is, $\phi' = 2.406 \times 10^{-05}$ (rad/cal). Equation (5) is used to predict the yaw behavior based on measured initial rates and angles.

A. First Magnitude of Yaw Effects

Total angle of attack versus distance downrange for a proof slug and a standard penetrator are shown in Figures (9a) and (9b). The results of using equation (5) to predict the yaw magnitude are also plotted. The data of Figure (9a) for the proof slug agree well with the behavior predicted by equation (5) since the slug was a full bore round with no discarding parts. Evidently muzzle blast effects can be ignored. The penetrator data shown in Figure (9b), however, diverge from the prediction of equation (5) after z = -1924.5 calibers. The penetrator data contain all the effects of the sabot discard disturbance and the figure shows the importance of taking these disturbances into account. From the Transonic Range round reduction, a first maximum yaw can be computed. For the penetrator, this yawing behavior is shown in Figure (10a) (dashed curve) and is compared to the prediction of equation (5) based on the muzzles rates. Also plotted for comparison are the data from the x-ray stations. The increase in first maximum yaw due to launch disturbances is clearly evident. The average first maximum yaws for the three different penetrator/sabot configurations are compared to the inbore predictions in the bar chart presentation of Figure (10b). The standard penetrator/sabot configuration showed the least inbore as well as discard effects. There is a progressive increase in both inbore and discard effects with the sub-borespan finned configuration and the penetrator/vented sabot assembly. The percentage of first maximum yaw due to discard disturbances is about 41% for each of the three types of test rounds.

B. Mechanical Separation

The test results show that mechanical separation plays an important role in the magnitude of observed initial yawing motion. Direct mechanical contact between sabot parts and the penetrator was maintained until the assembly reached station two. (Figure (5a-b)). Between stations two and three, mechanical separation took place as seen in Figures (5b-c). Beyond station three the discard interaction was purely aerodynamic. The photographic evidence suggests that only a single mechanical interaction took place between stations two and three. Using the angular information at station two and first-order differences between stations two and three to obtain rates, initial values for equation (5) were computed and a yaw behavior predicted. This new yaw behavior was analyzed to yield a first maximum yaw value which is due to both the angular momentum produced by mechanical interaction as well as the angular momentum resident in the system at station two. Figure (11a) shows all three contributions to the first maximum yaw: inbore, mechanical, and aerodynamic.

The penetrator was in free flight past station five as seen in Figures (5e-f). Figure (5e) shows the sabot petals sufficiently far removed from the penetrator to provide any intersecting shocks with the penetrator tail. Figure (5f) shows that the sabot shocks were behind the penetrator. Data from

stations five and six were included in the range reduction. Although the range reduction did not predict the correct location of the x-ray free flight data, Figure (11a), the angular rate of the x-ray data at stations five and six were reasonably well predicted. Beyond station three, strong shock interactions between sabot petals and the penetrator provided the final discard disturbances. The momentum exchange due to aerodynamic discard effects brought the angular momentum of the penetrator to a level compatible with that indicated by the first maximum yaw extrapolation from the range reduction. The bar chart of Figure (11b) illustrates the contribution of each of the effects, inbore, mechanical, and aerodynamic, to the average first maximum yaw for each penetrator/sabot type. The Figure shows that the mechanical separation effects were "favorable" for the penetrator with sub-borespan fins and the penetrator with the vented sabot petals but were larger in magnitude than for the standard penetrator. The aerodynamic interaction was least for the standard penetrator and greatest for the penetrator/vented-sabot configuration. The adverse aerodynamic effect for the penetrator/vented-sabot case was due to the longer discard interaction times of the vented sabots.

V. ANALYSIS

The analysis of the preceding section gives an overall view of the interaction between discard disturbances and the penetrator and shows how the interaction changes the initial angular momentum to the free flight value. The penetrator with vented sabot petals has the greater total first maximum yaw despite the "favorable" mechanical interaction. The term "favorable" is meant to indicate a reduction in first maximum yaw. It should be made clear that any discard interaction which causes the penetrator to deviate from its original yaw behavior is undesirable.

A more detailed investigation of the discard sequence can be made if a baseline for comparison is available. Inasmuch as there is no control over inbore effects, we select the yaw predicted by the measured angular rates at the muzzle as the baseline. This baseline, then, is the curve in Figure (11a) labeled "inbore effects." Each test round fired had different initial conditions at the muzzle. Therefore, in order to compare the results from different rounds, it is necessary to normalize the results in such a way that they are either in a common reference frame or are presented relative to the baseline. Equation (5) can be rewritten in the following form:

$$\eta = [\tilde{\xi} - \tilde{\xi}_0 \cos(\phi' S)]/(\tilde{\xi}_0'/\phi') = \sin(\phi' S). \tag{7}$$

Equation (5) can be decomposed into real and imaginary parts and is normalized just as was equation (7):

$$\eta_\alpha = [\tilde{\alpha} - \tilde{\alpha}_0 \cos(\phi' S)]/(\tilde{\alpha}_0'/\phi') = \sin(\phi' S). \tag{8a}$$

$$\eta_\beta = [\tilde{\beta} - \tilde{\beta}_0 \cos(\phi' S)]/(\tilde{\beta}_0'/\phi') = \sin(\phi' S). \tag{8b}$$

The magnitude of Equation (7) is:

$$|n| = |[\tilde{\xi} - \tilde{\xi}_0 \cos(\phi' S)]/(\tilde{\xi}_0'/\phi')| = |\sin(\phi' S)|. \quad (9)$$

We will refer to $|n|$ as the normalized yaw. Thus, the equation describing the yawing motion of a round in free flight has been recast in normalized form so that all rounds in free flight are described by a single curve independent of launch conditions. This procedure is akin to writing boundary layer equations in similarity coordinates. The pertinent similarity variables here are $|n|$ and $\phi' S$. Thus, the free flight yaw behavior is scaled in amplitude, $0 \leq |n| \leq 1$, and in frequency, $0 \leq \phi' S \leq 2\pi$. The normalization has removed the inbore or initial effects and the free flight motion of all penetrators is described by:

$$|n| = |\sin(\phi' S)|. \quad (10a)$$

The test data can then be used to evaluate:

$$|n| = |[\tilde{\xi} - \tilde{\xi}_0 \cos(\phi' S)]/(\tilde{\xi}_0'/\phi')|. \quad (10b)$$

$$|n| = \{[\tilde{\beta} - \tilde{\beta}_0 \cos(\phi' S)]^2 + [\tilde{\alpha} - \tilde{\alpha}_0 \cos(\phi' S)]^2\}^{1/2}/\{(\tilde{\beta}_0'^2 + \tilde{\alpha}_0'^2)/\phi'^2\}^{1/2}. \quad (10c)$$

Any difference between the test data and Equation (10a) is a measure of the effects of the discard loadings only.

A plot of $|n|$ versus $\phi' S$ is given in Figures (12a-b) for the standard penetrator, in Figure (12c) for the penetrator with the sub-borespan fins, and in Figure (12d) for the penetrator/vented sabot configuration. The standard penetrator is seen to have the greatest discard disturbances. The penetrator with the sub-borespan fins seems to have the least discard disturbances. Both the penetrator with sub-borespan fins and the penetrator/vented sabot show significantly less discard disturbances than the standard penetrator. This statement appears to contradict the statements made about Figure (11b). In the normalized system, the discard disturbances are measured relative to the inbore effects and consequently a strong discard disturbance does not necessarily result in poor overall performance.

Figures (12a-b) include a significant amount of data for the standard penetrator. Within certain tolerances, one standard penetrator/sabot round is identical to the next and all rounds were fired from the same gun. Nevertheless, the discard disturbances range from weak to strong. If the discard disturbances were symmetric, one would not expect the firing data to deviate from the predictions of Equation (10a). The data, however, do differ, and, the greater the difference, the more asymmetric the discard disturbance. The

asymmetry is found in the initial conditions at the muzzle of the gun. While in the gun tube, the round experiences a periodic motion known as inbore balloting. A planar description of balloting is shown in Figure (13). The penetrator/sabot shot center of gravity moves toward and away from the axis of the tube and the shot yaws about its center of gravity. The sabot components which constrain the penetrator to move along the tube axis can be modeled by two stiff springs. As the shot ballots in the tube, the sabots elastically expand and compress. At muzzle exit, the sabots can be elastically stressed between two limiting states. Either one sabot component is highly stressed and the other is relaxed or both sabot components are equally stressed.

If the inbore behavior is assumed periodic, and given by a cosine law, we can write:

$$\varepsilon = A \cos(\omega t + \phi_0) \tag{11a}$$

where ε is the angle the penetrator makes with the tube axis. The rate at which the penetrator/sabot shot ballots is:

$$\dot{\varepsilon} = -\omega A \sin(\omega t + \phi_0). \tag{11b}$$

The angular orientation of the package inbore is uniquely described by ε and $\dot{\varepsilon}$. The balloting amplitude can be eliminated by taking the ratio of Equations (11a) and (11b):

$$\dot{\varepsilon}/\varepsilon = -\omega \tan(\omega t + \phi_0) \tag{11c}$$

which describes the system in terms of the balloting frequency, ω, and an initial condition, ϕ_0. For a given system, the balloting frequency, ω, is a function of the system geometry. The initial condition is indeterminate and varies with shot start at the breech of the gun. The length of time, t, the shot is in the gun is a function of tube length and shot velocity. For a given tube and fixed charge, t does not vary significantly from one shot to the next. Thus, ϕ_0 is responsible for the variations in $\dot{\varepsilon}/\varepsilon$ and this ratio is a measure of the state of stress of the sabot components.

At the peak of the balloting motion, $\dot{\varepsilon}$ goes to zero and, consequently, $\dot{\varepsilon}/\varepsilon$ goes to zero. At this point in the motion, one sabot component is more highly stressed than the other. Conversely, the point of equal sabot stresses occurs at the maximum angular rate with the balloting angle equal to zero, that is, as $\dot{\varepsilon}/\varepsilon$ goes to infinity. The elastic decompression of sabot components starts the discard sequence and is the mechanism by which asymmetry in the gun tube is transferred to the discard sequence. If $\dot{\varepsilon}/\varepsilon$ is a measure of

asymmetry at tube exit, it should correlate with the severity of the discard interaction. The x-ray data provide the muzzle angular rates and angles. Let us describe the severity of the discard by the parameter Δn, the magnitude of the difference of the data from the behavior predicted by Equation (10a), Figure (12). Figure (14b) is a plot of $|\Delta n|$ versus δ_0'/δ_0, the absolute value of $\dot{\varepsilon}/\varepsilon$. Only rounds with data at station six are included in the plot. All the rounds with large discard disturbances are grouped near zero. These rounds exit the tube with one or more of the sabot petals highly stressed in an asymmetric fashion. Of greater significance, however, is that there exists a region beyond which the discard disturbances are a minimum. Note that the nonstandard penetrator/sabot packages were launched with δ_0'/δ_0 on the borderline or beyond the point where the discard disturbances approach a minimum value.

The quantity $|\Delta n|$ is an accurate measure of the launch disturbance only if evaluated in the neighborhood of first maximum yaw where it directly relates to the total work done on the penetrator. Evaluated away from first maximum yaw, $|\Delta n|$ can be related only to that part of the total work done before first maximum yaw. Thus far, $|\Delta n|$ is only a measure of the difference of the data from the yaw behavior predicted by the initial conditions at the muzzle. Since the discard not only alters the level but also displaces the position of first maximum yaw, it is not clear how close the data are to the first maximum yaw. The correlation of Figure (14b) may be fortuitous because of this consideration. The paucity of data is an additional problem in evaluating the correlation. In future tests, data must be obtained at first maximum yaw. At values of δ_0'/δ_0 where large discard disturbances were evident, data also existed for rounds with small disturbances. Thus, a low value of δ_0'/δ_0 is a necessary but not sufficient condition for large discard disturbances. There are other conditions which comprise a sufficient set and what they consist of is a topic for further research.

Schmidt and Shear[4] have obtained penetrator yaw data for a 60mm sabot-penetrator combination. The sabot design is similar to that for the present test rounds with the exception that the front lifting surface does not have the extended cup. The rounds of Reference 4 were fired from a rifled tube while the rounds of this report were fired from a smooth bore tube. The 60mm round has an initial roll rate of 110 rev/sec and uses centrifugal acceleration together with aerodynamic loads to throw off the sabot components. The data from Reference 4 can be analyzed in the same way as the data from the smooth bore firings. The normalized yaw, n, is redefined to include the effects of roll. The following yaw equation applies for the rolling case:

$$\tilde{\xi} = [\tilde{\xi}_0'/(i(\phi_1' - \phi_2'))][e^{i\phi_1' S} - e^{i\phi_2' S}] + [\tilde{\xi}_0/(\phi_1' - \phi_2')][\phi_1' e^{i\phi_2' S} - \phi_2' e^{i\phi_1' S}] . \quad (12a)$$

The magnitude of the normalized yaw is defined as:

$$|n| = \left| \frac{\tilde{\xi} - \tilde{\xi}_0 \left[\phi\hat{1} e^{i\phi\hat{2}S} - \phi\hat{2} e^{i\phi\hat{1}S}\right]/(\phi\hat{1} - \phi\hat{2})}{\left[\tilde{\xi}_0'/(i(\phi\hat{1} - \phi\hat{2}))\right]} \right| = \left| e^{i\phi\hat{1}S} - e^{i\phi\hat{2}S} \right|. \quad (12b)$$

The fast and slow frequencies, $\phi\hat{1}$ and $\phi\hat{2}$, may be evaluated from:

$$\phi\hat{j} = (1/2)\left[iP \pm (4M - P^2)^{1/2}\right]. \quad (13a)$$

$$M = \left[\rho A d^3/(2I_y)\right] Cm_\alpha. \quad (13b)$$

$$P = (pd/V)\ (I_x/I_y). \quad (13c)$$

The downrange similarity variable in this coordinate system is now $(\phi\hat{1} - \phi\hat{2})S$. The data are evaluated using the first equality in Equation (12b) and the prediction is computed using the second equality in Equation (12b). Figure (15) shows a comparison of the data from the standard penetrator of this report with the data from Reference 4. The effects of the discard disturbances are quite similar. In both tests, the data differ from the similarity prediction. Just as for the standard round of this report, Figure (12a), a variety of discard disturbances are evident for the data of Reference 4. Let us define $|\Delta n|$ as before, and correlate the Reference 4 data with initial δ_0'/δ_0. Figure (16) shows that the data of Schmidt and Shear appear to have the same type of relationship to initial conditions as the present case. The results are plotted in the coordinate system of Equations (12) so that both sets of data are properly scaled relative to each other. Only five data points are available from Reference 4 and hard conclusions cannot be made. The proper trend, however, is indicated.

The analysis thus far has considered the effects of the discard process on the total yaw. If the discard disturbances are not a function of the yawing motion of the penetrator then the perturbations to the total yaw are a good measure of the discard effects. However, should the yawing motion of the penetrator and the discard loads be coupled, then a similar analysis can be used on the components of yaw. It is possible to construct the effects of discard on the components of yaw, that is on the pitching and yawing motions considered separately. The components of yaw, the angle of attack, and the angle of sideslip are not necessarily similar in amplitude and the discard disturbances are not necessarily in either plane. Equations (8) have already been developed to provide expressions for normalized yaw in both the pitch and yaw planes. Let us begin by considering the proof slug. The proof slug has no discarding sabot, hence no discard disturbance, and its components of yaw, n_α and n_β, should correlate with the predictions of Equations (8). Figure (17a) shows the results of a comparison of $|n_\alpha|$ and $|n_\beta|$ with the magnitude of the

second equality of Equations (8) and it is seen that the data agrees with the prediction and behaves the same for either function.

For the sabot/penetrator packages, a variety of disturbances are possible. Figure (17b) gives an example of a discard disturbance acting in the α plane only. Figure (17c) shows a small disturbance in either plane. Figure (17d) illustrates equal discard disturbances in both α and β planes. In Figure (17e) we see an "unfavorable" disturbance in the α plane and a "favorable" disturbance in the β plane. Finally, in Figure (17f), we see almost no discard disturbance in the α plane and a substantial disturbance in the β plane. Figure (18a) shows the result of plotting the yaw predictive equation (5) as well as the standard penetrator data in the α - β plane. The yaw prediction is the usual ellipse while the data seem to show planar motion. On the other hand, Figure (18b) shows a planar prediction while the data exhibit non-planar behavior due to the discard process.

For a non-rolling projectile, the pitch and yaw equations are uncoupled. If the discard phenomenon is not a function of the angular motion of the penetrator, then the disturbances can be resolved into α and β components and the equations remain uncoupled. If we assume this to be the case, we can define $|\Delta n_\alpha|$ and $|\Delta n_\beta|$ in a fashion similar to $|\Delta n|$, Figure (17d). The correlations for the discard disturbances in the α and β planes are given in Figures (19a-b). These correlations are not as pronounced as the correlation for the total disturbance, $|\Delta n|$. This leads to the conclusion that for this round the discard disturbances may be weakly coupled to the yaw behavior of the penetrator. Nevertheless, the evidence supports the contention that the largest discard disturbances occur for low values of α_0'/α_0 or β_0'/β_0.

VI. SUMMARY

A series of firing tests of standard penetrators, penetrators with sub-borespan fins, and penetrators with vented sabot petals was conducted to provide data relevant to the sabot discard process. Analysis of the test results shows that it is possible to quantify the magnitude of the inbore, mechanical, and aerodynamic contributions to the total discard disturbance. Gross effects of the discard disturbances can be readily determined from the firing results, as seen in Figure (11b). A full-bore round experiences only inbore effects while sub-bore penetrator/sabot rounds experience severe discard disturbances. The discard disturbances lead to increases in first maximum yaw of about 41% for the standard penetrator. The vented sabot/penetrator packages and the sub-borespan fin penetrators also have a net increase in first maximum yaw of about 41%, but the discard effects contributed more strongly to the first maximum yaw increase.

Penetrator/vented sabot packages showed increased inbore effects over the standard penetrator/sabot configurations. Inbore, the standard penetrator, is the most stable since it has a front borerider as well as a rear borerider, the fin assembly. The penetrators with sub-borespan fins lose the rear borerider stability and an increase in inbore effects is noticed. If the inbore contribution of the standard penetrator is used as a baseline for comparison, then the loss of the rear borerider gives about 50% increased inbore contribution. The vented sabot/penetrator packages produced about 100% increase in

the inbore contribution. Venting the sabots may eliminate initial aerodynamic lift but the structural response of the front boreriding system is also changed. Since the penetrators with vented sabots also had boreriding fins, it is clear that the structural design of the front boreriding system is critical to the inbore behavior. Indeed, the front boreriding design seems much more important than the rear boreriding fins. The front boreriding system could be structurally stiffened to upgrade inbore performance. The result should be levels of first maximum yaw comparable to those of the standard penetrator. A series of such experiments is recommended since the payoff would be improved terminal penetrator performance with higher accuracy.

The purpose of the vented sabot/penetrator tests was to relieve the mechanical interaction between penetrator and sabot. Although the mechanical interaction changed from "unfavorable" to "favorable." it did not reduce the magnitude of the interaction, but rather increased it. A change in the first maximum yaw is produced by an angular impulse which is an integrated quantity. The increase in discard time was enough to increase the magnitude of the impulse even though the applied moment may have actually decreased. The effect of increased discard time is also evident from the increased aerodynamic disturbance to the penetrators with the vented sabot package. The AVCO sabot discard code[8] predicted a reduction in the level of the mechanical impulse for the vented sabot/penetrator package. It is clear from the data that this was not the case. The AVCO code computations were based on a symmetric discard of the sabot components. A computation including the asymmetric effects on the discard is needed for a proper comparison. Such a computation is presently being performed.

A simple model of the inbore behavior of sabot/penetrator combinations allowed a correlation between the severity of the discard and the initial conditions at the muzzle. From these correlations, Figures (14b), (19a-b), it can be seen that sabot/penetrator combinations with small initial δ_0'/δ_0 ratios (related to an asymmetrically compressed state) are characterized by large discard disturbances. There is a point beyond which the discard disturbances appear to diminish to a constant level.

The aerodynamic dispersion of a full bore round is related to the angular rate at the muzzle. Improved performance of full bore rounds can be achieved by reducing the initial angular rates. For sabot/penetrator combinations, such a strategy could lead to increased discard disturbances, offsetting any gains achieved by reducing the initial angular rates. Thus, the optimal launch point for APFSDS ammunition is at values of δ_0'/δ_0 beyond the point where discard disturbances manifest themselves (i.e. at a δ_0'/δ_0 of 0.015 in Figure (14b) for the present case) and at the least possible angular rate for a minimum inbore launch disturbance.

VII. CONCLUSIONS

1. The net increase in first max yaw associated with sabot discard disturbances averages 41% for all APFSDS rounds tested.

2. The inbore contribution to first maximum yaw of a long rod penetrator may be reduced by stiffening the front borerider.

3. The severity of the discard disturbances can be correlated to the initial conditions at the muzzle.

4. Sabot/penetrator combinations launched in an asymmetrically compressed state are characterized by increased discard disturbances.

5. There is an initial angular rate to angle ratio beyond which the discard disturbances asymptote to the constant level.

6. APFSDS ammunition should be launched at angular rate to angle ratios large enough so that the discard disturbances do not manifest themselves and at angular rates producing the minimum inbore launch disturbance.

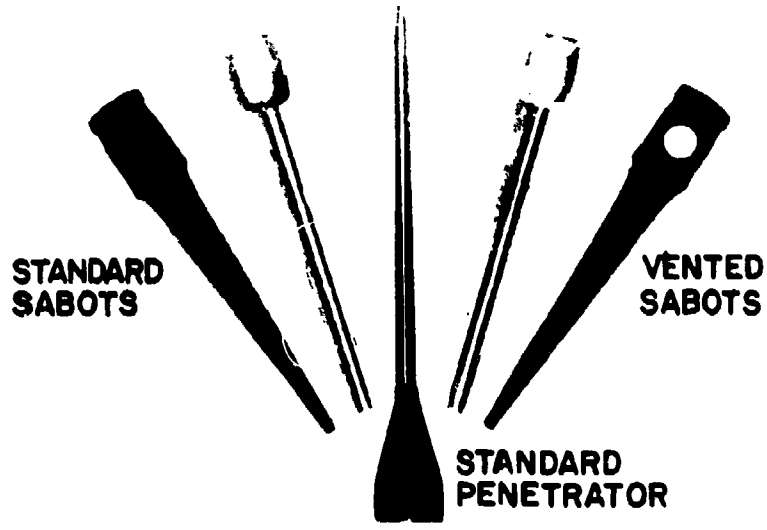

FIG. (1) TEST ROUND AND SABOTS

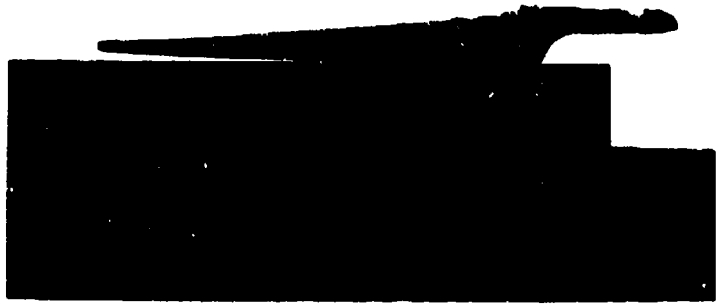

FIG. (2) BENT SABOT

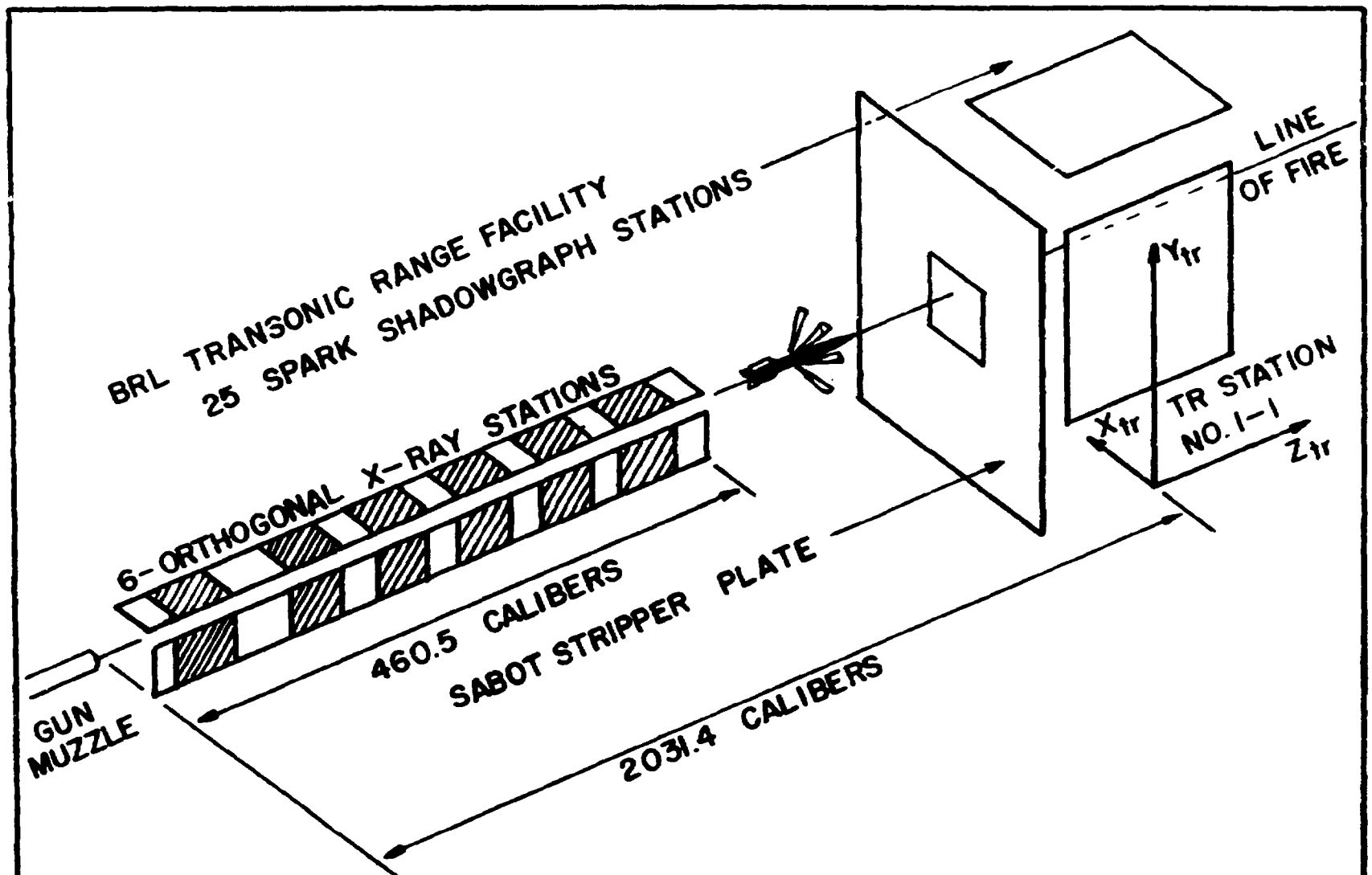

FIG.(3) SCHEMATIC OF THE TEST RANGE

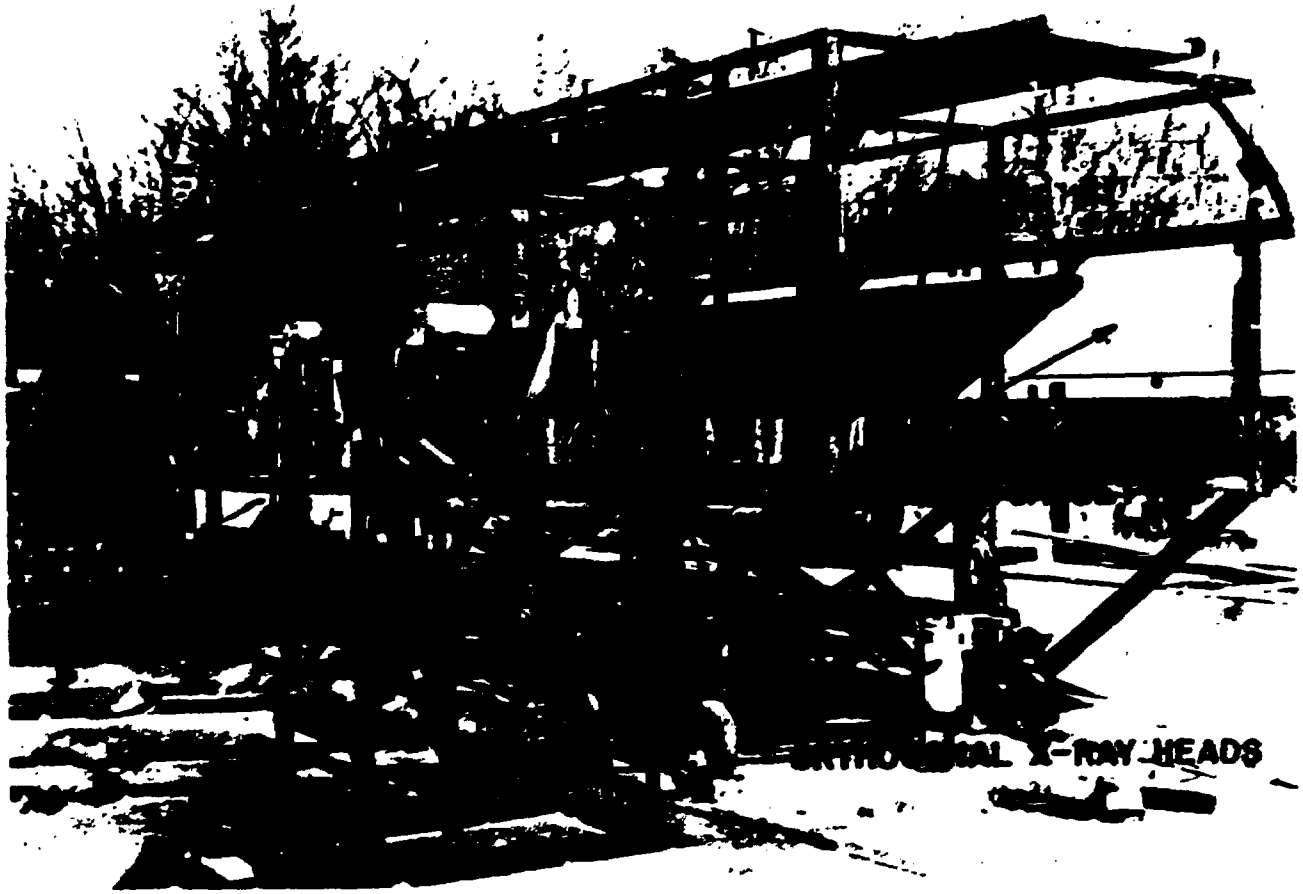

FIG.(4) ORTHOGONAL X-RAY APPARATUS

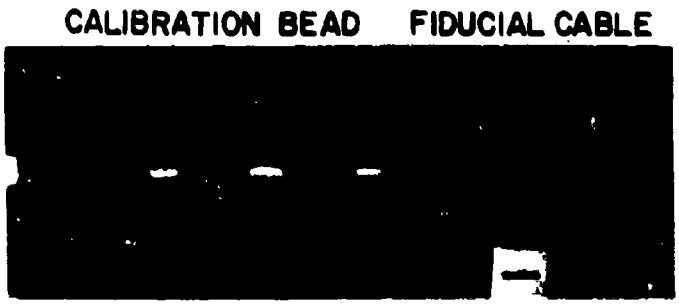

(5a) MUZZLE EXIT

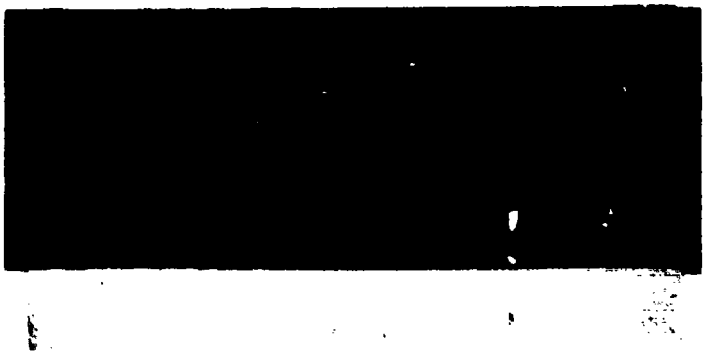

(5b) MECHANICAL INTERACTION

FIG.(5) DISCARD SEQUENCE X-RAY DATA

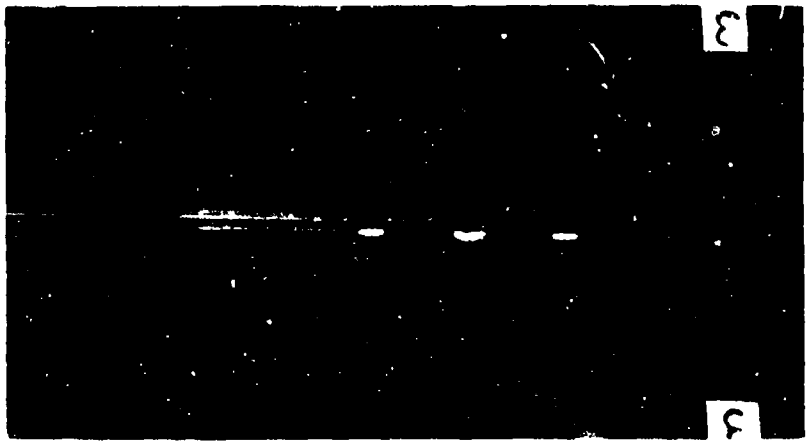

(5c) SABOT SEPARATION

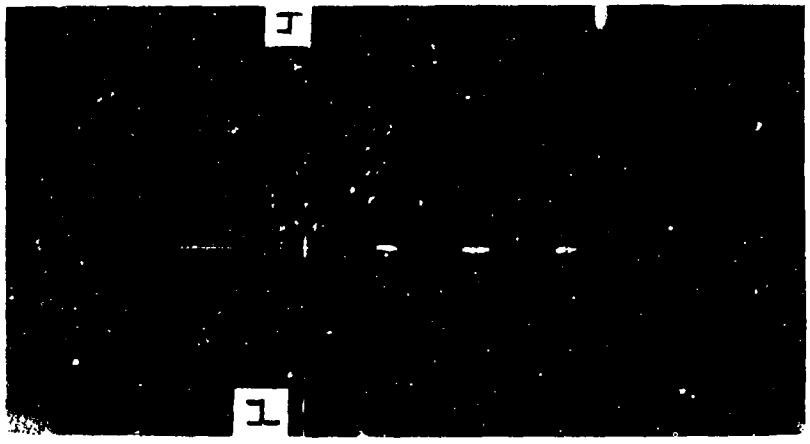

(5d) AERODYNAMIC INTERFERENCE

FIG.(5) CONTINUED

(5e) INITIATION OF PENETRATOR FREE FLIGHT

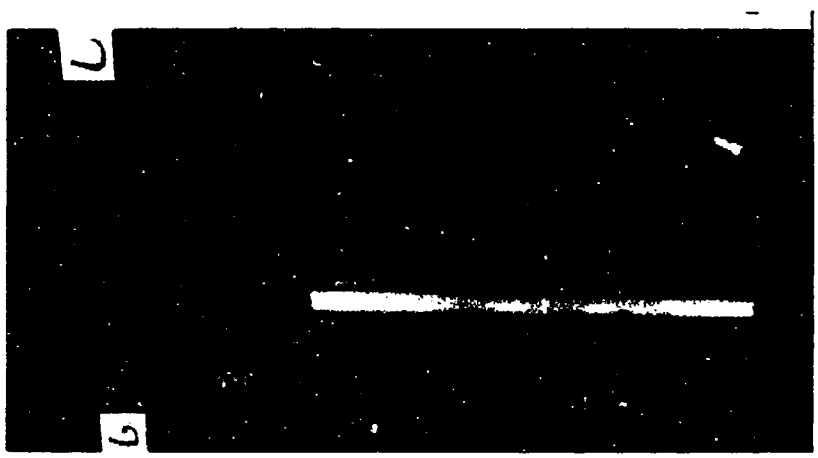

(5f) FREE FLIGHT

FIG.(5) CONTINUED

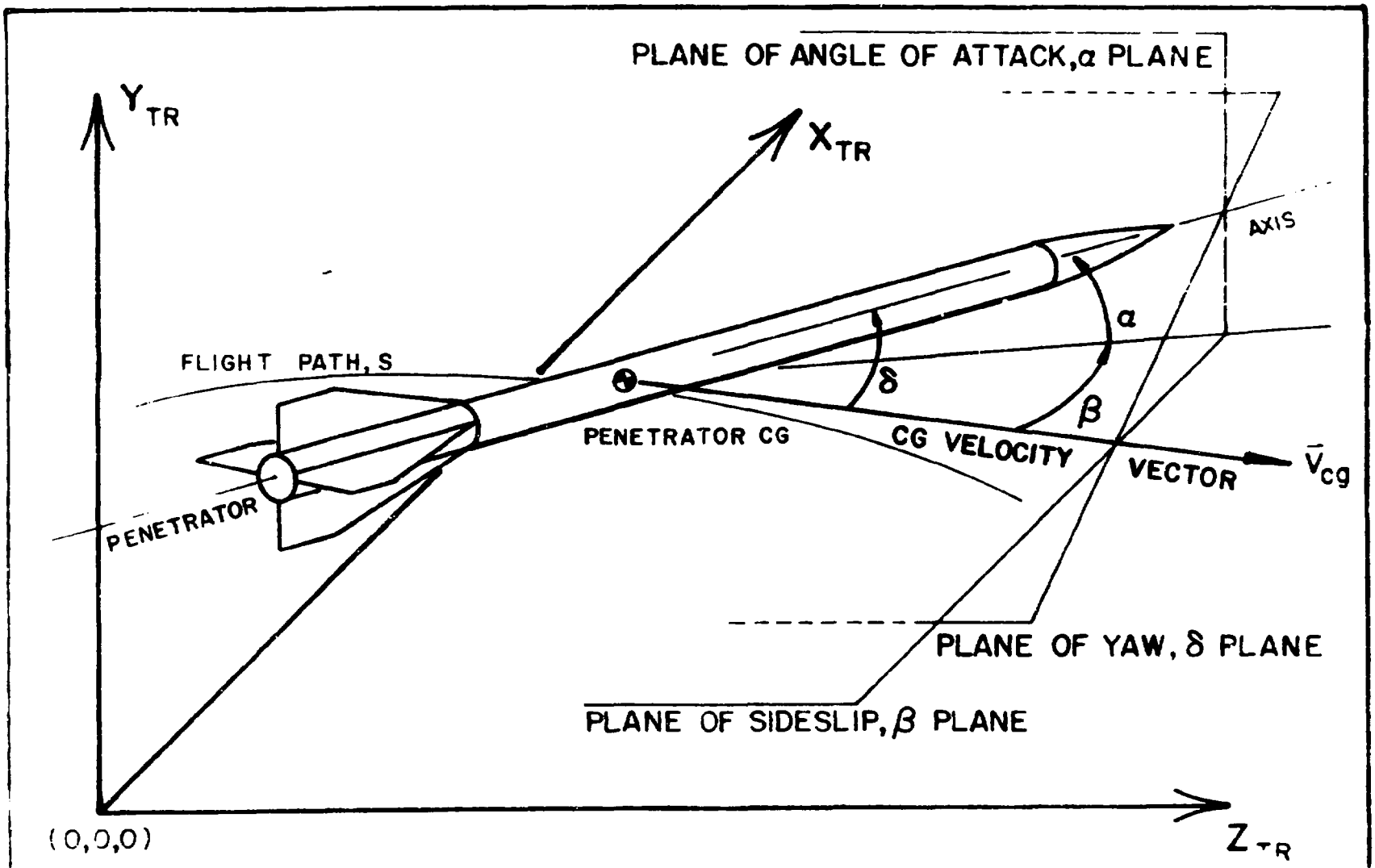

FIG. (6) PENETRATOR COORDINATE SYSTEM

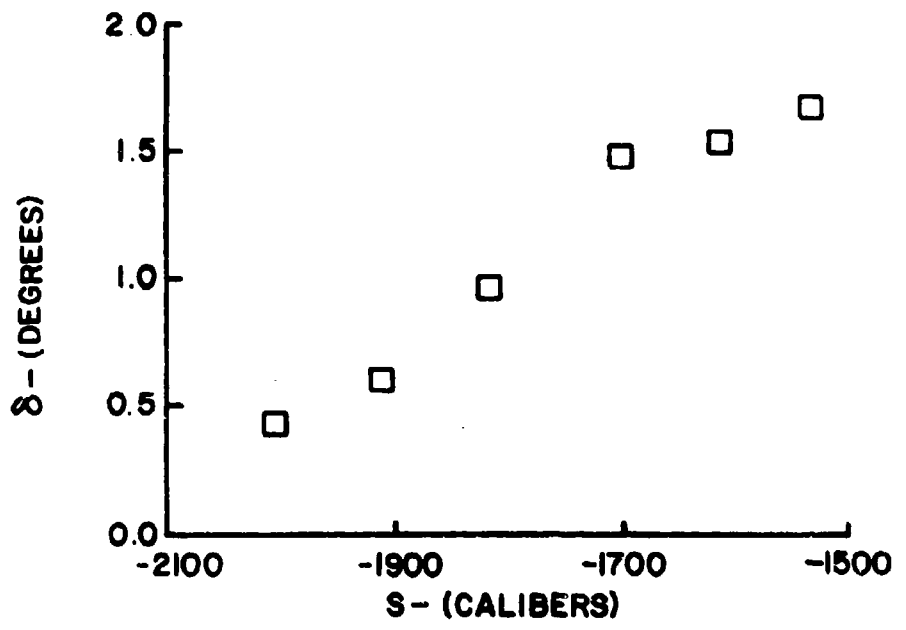

(7a) MAGNITUDE OF YAW

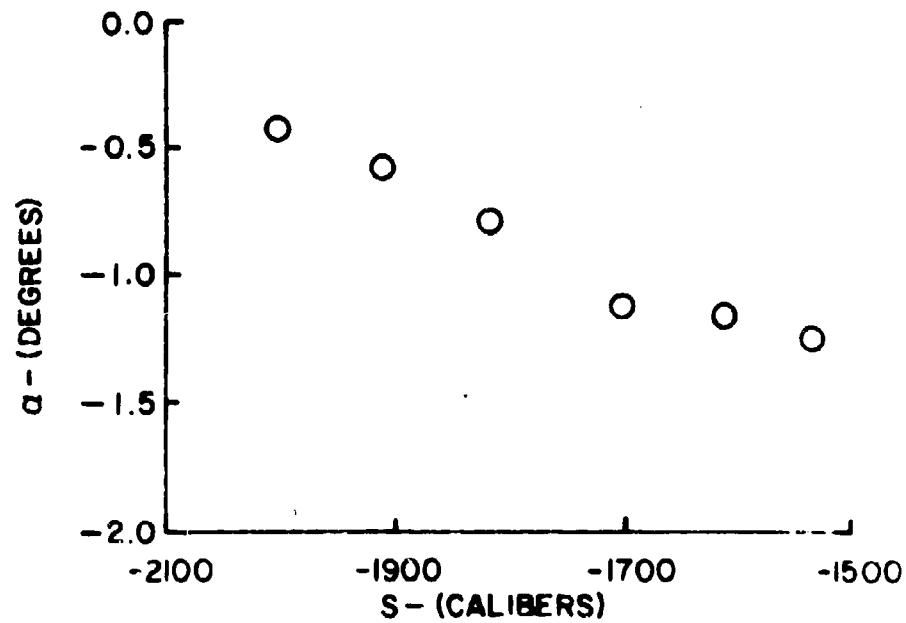

(7b) ANGLE OF ATTACK

FIG. (7) ANGULAR X-RAY DATA STANDARD PENETRATOR

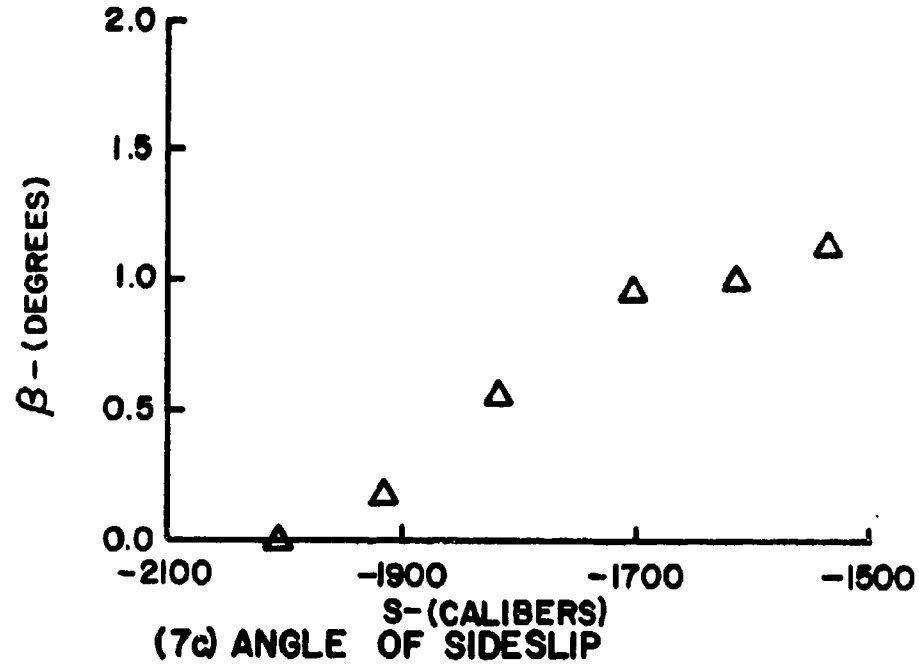

(7c) ANGLE OF SIDESLIP

FIG.(7) CONTINUED

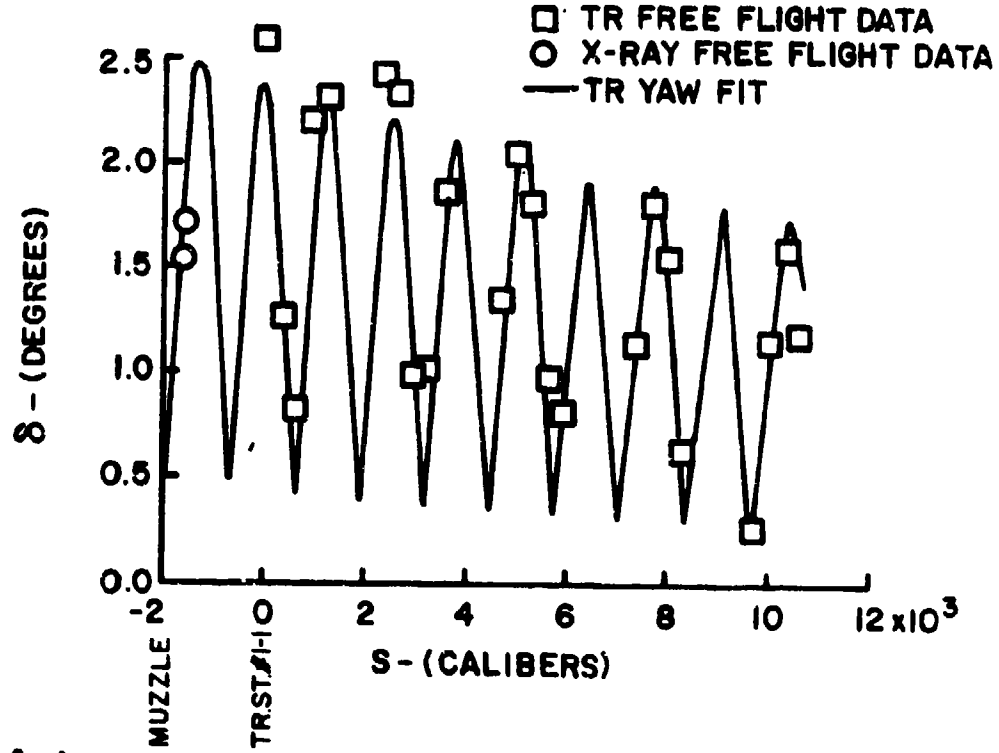

FIG.(8) TRANSONIC RANGE YAW FIT

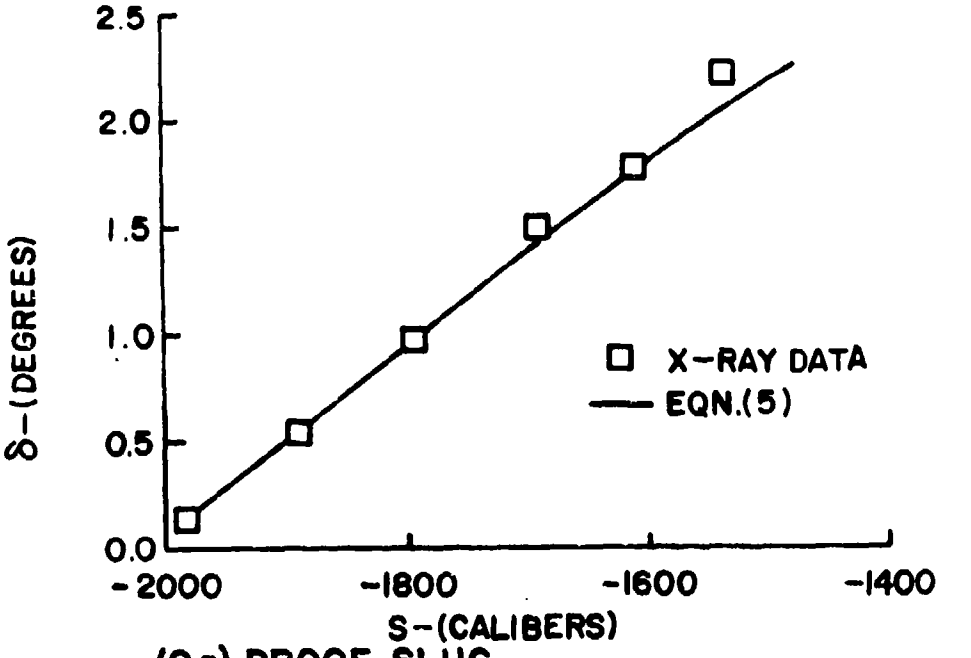

(9a) PROOF SLUG

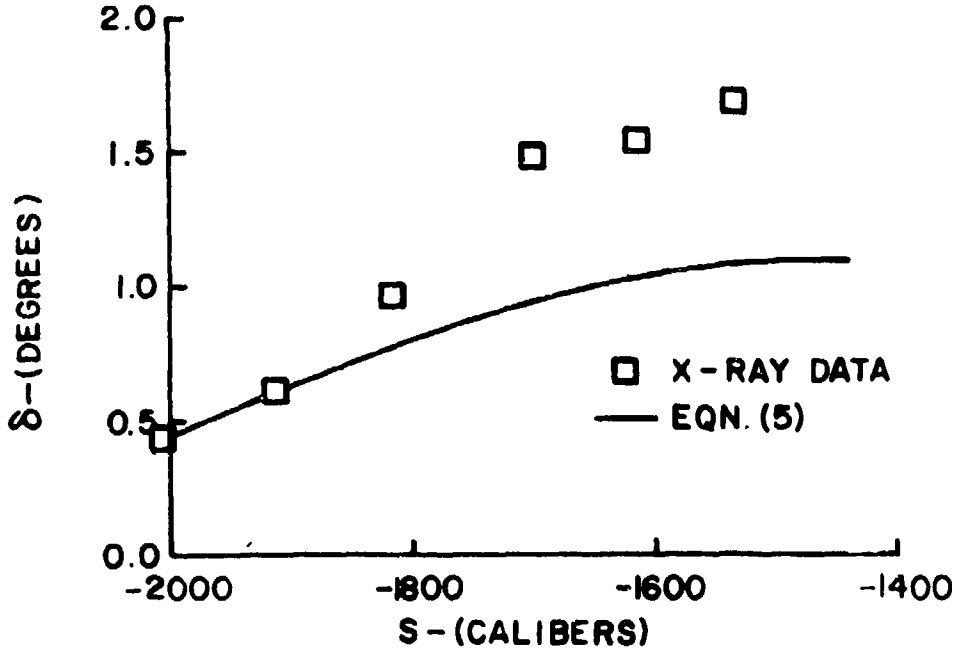

(9b) STANDARD PENETRATOR

FIG.(9) COMPARISON OF X-RAY DATA TO YAW PREDICTION

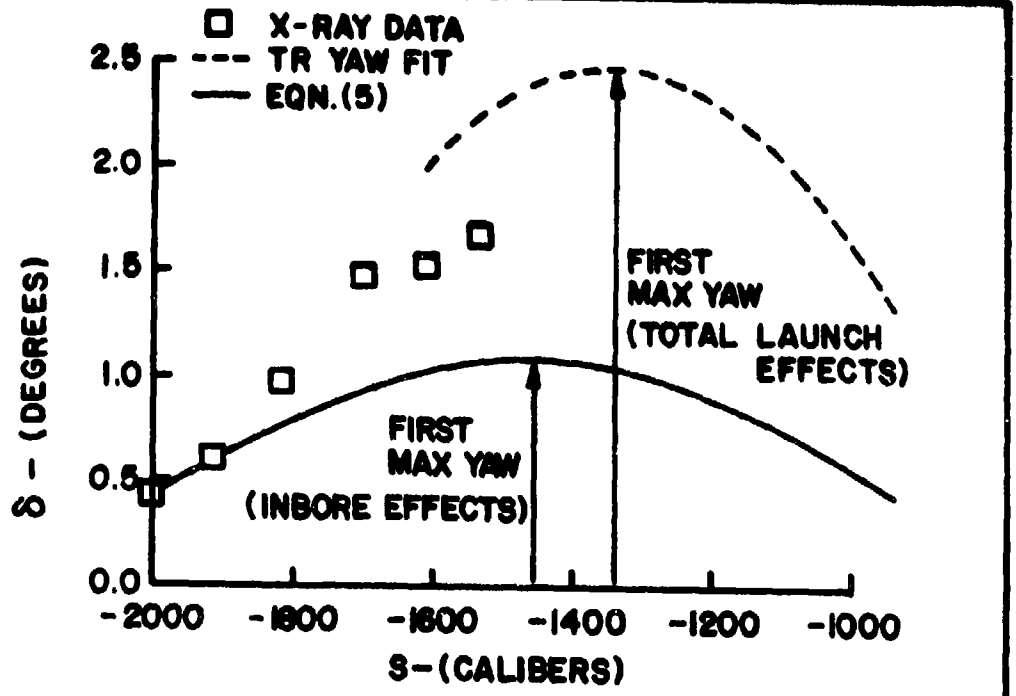

(10a) DEFINITION OF FIRST MAX YAW

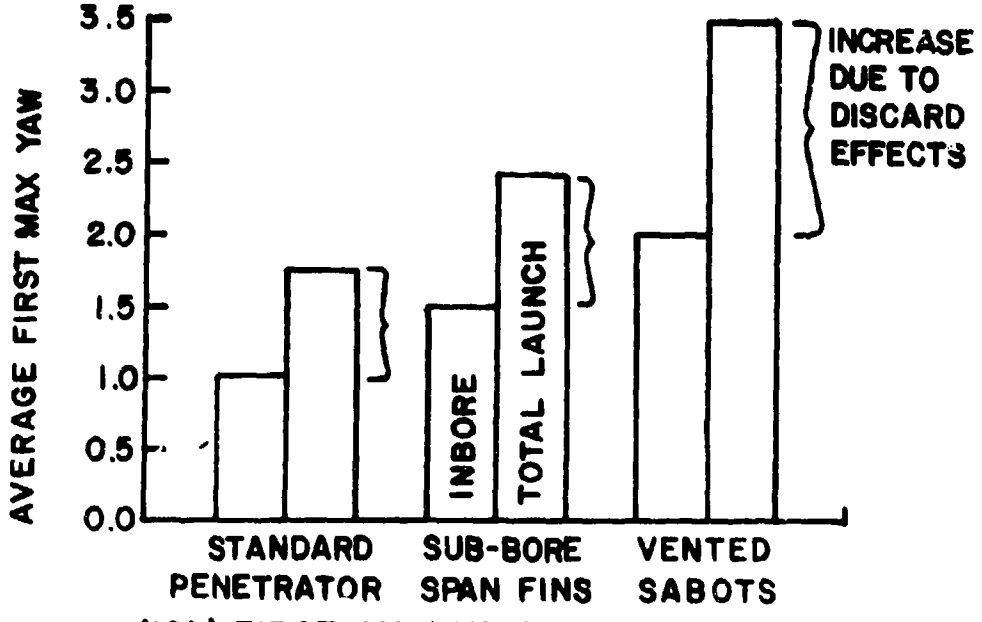

(10b) FIRST MAX YAW SUMMARY

FIG.(10) INCREASE IN FIRST MAX YAW DUE TO DISCARD DISTURBANCES

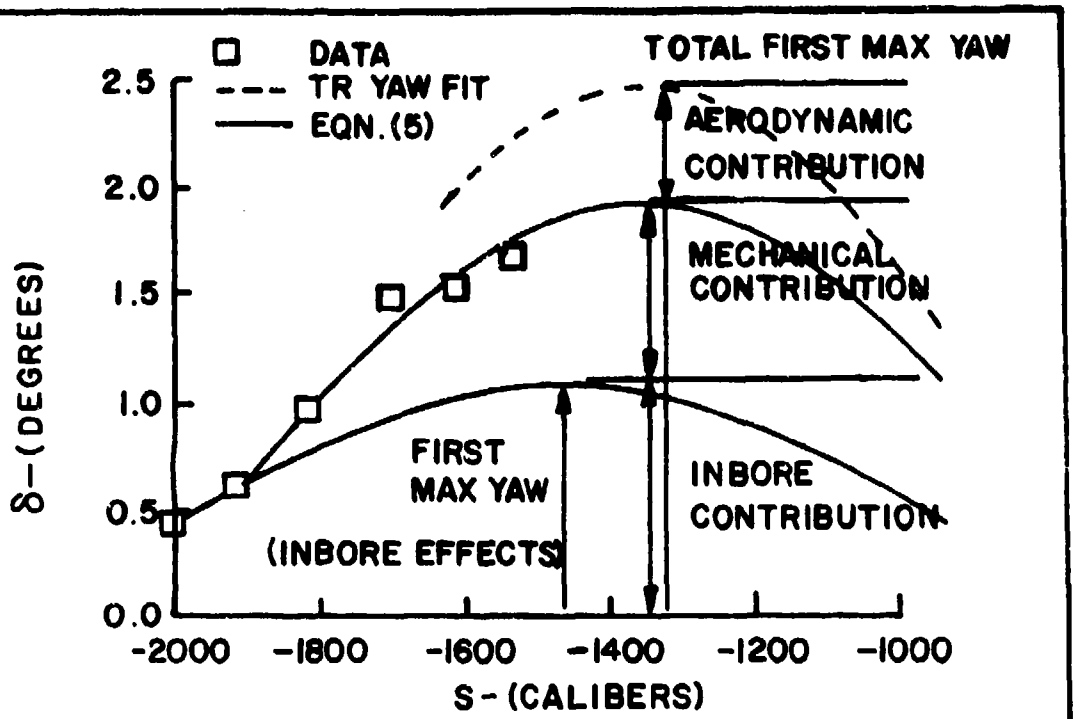

(11a) COMPOSITION OF FIRST MAX YAW

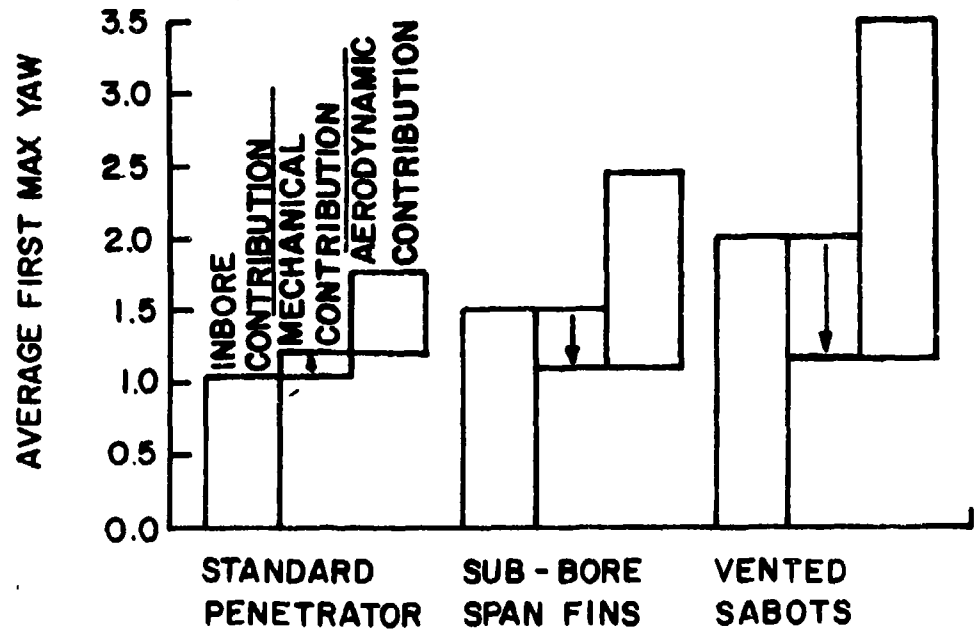

(11b) SUMMARY OF THE COMPOSITION OF FIRST MAX YAW

FIG.(11) COMPOSITION OF FIRST MAX YAW

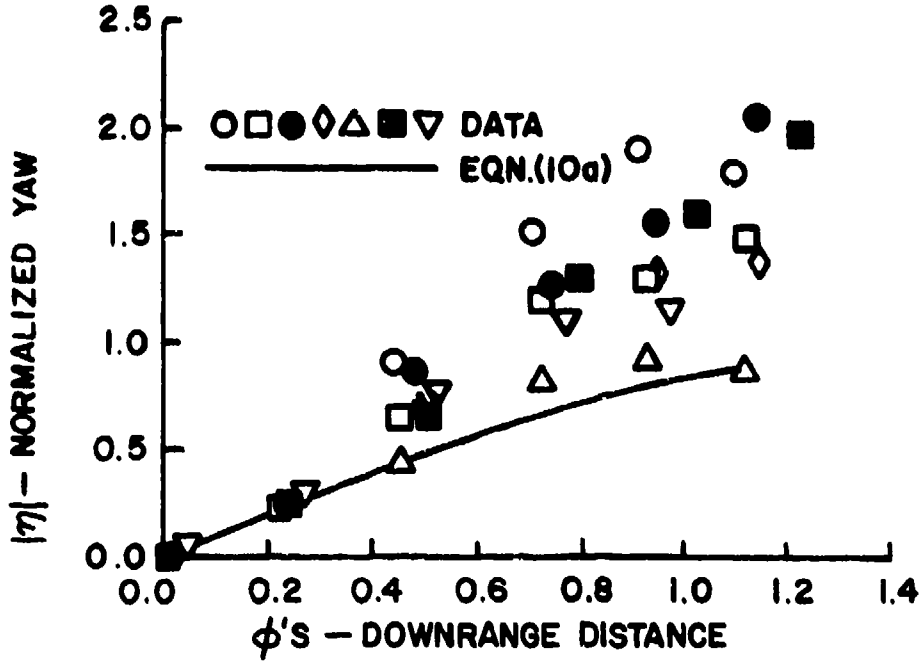

(12a) STANDARD PENETRATOR RD.#S'. 1–7

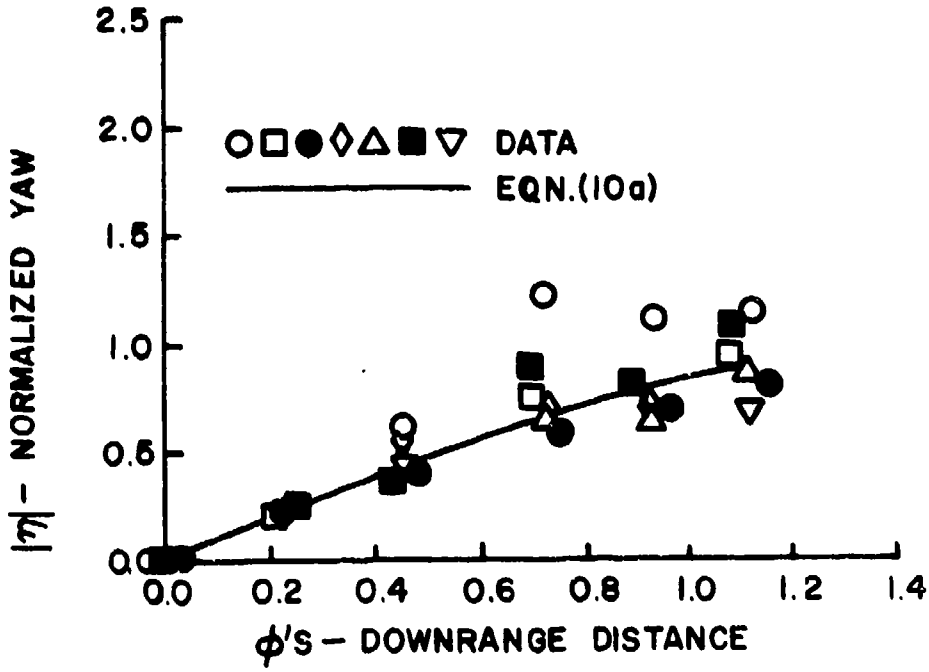

(12b) STANDARD PENETRATOR RD.#S'. 8–14

FIG.(12) NORMALIZED YAW VS. DOWNRANGE DISTANCE SIMILARITY COORDINATES

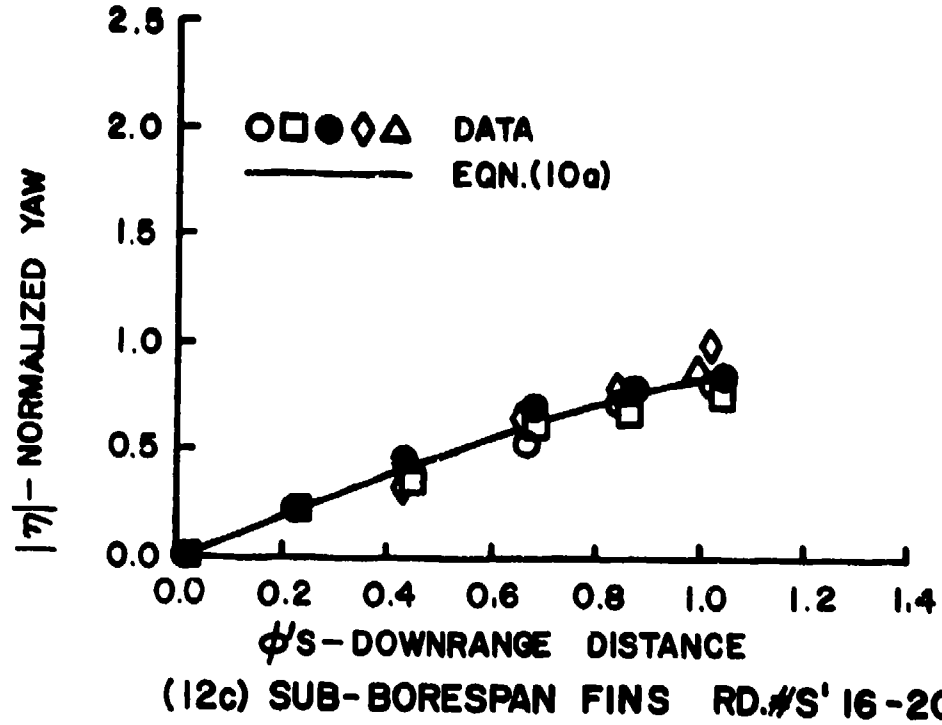

(12c) SUB-BORESPAN FINS RD.#S' 16-20

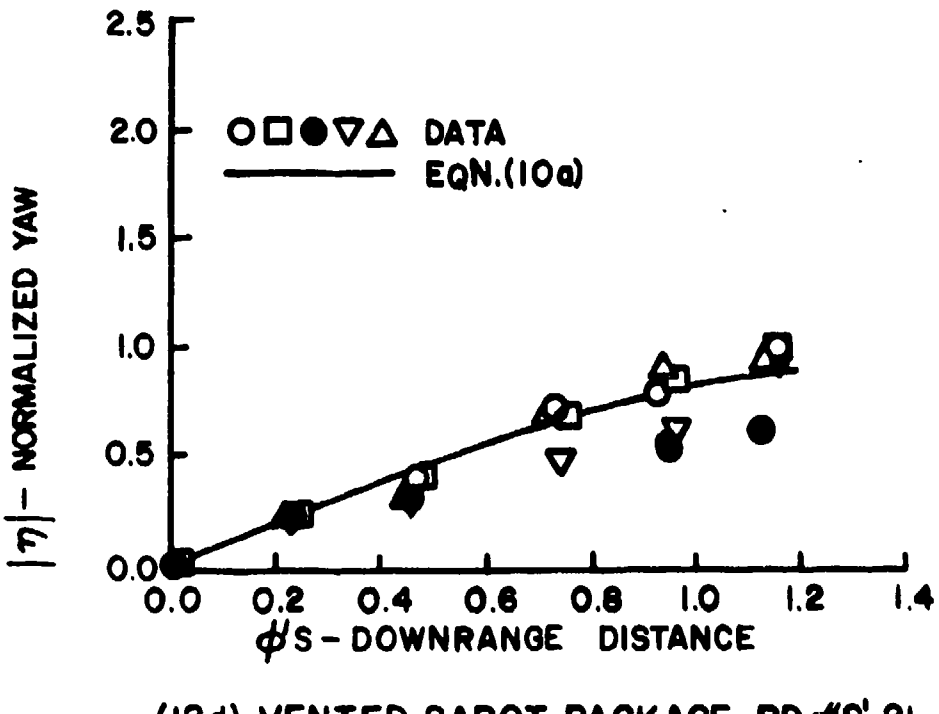

(12d) VENTED SABOT PACKAGE RD.#S' 21-25

FIG. (12) CONTINUED

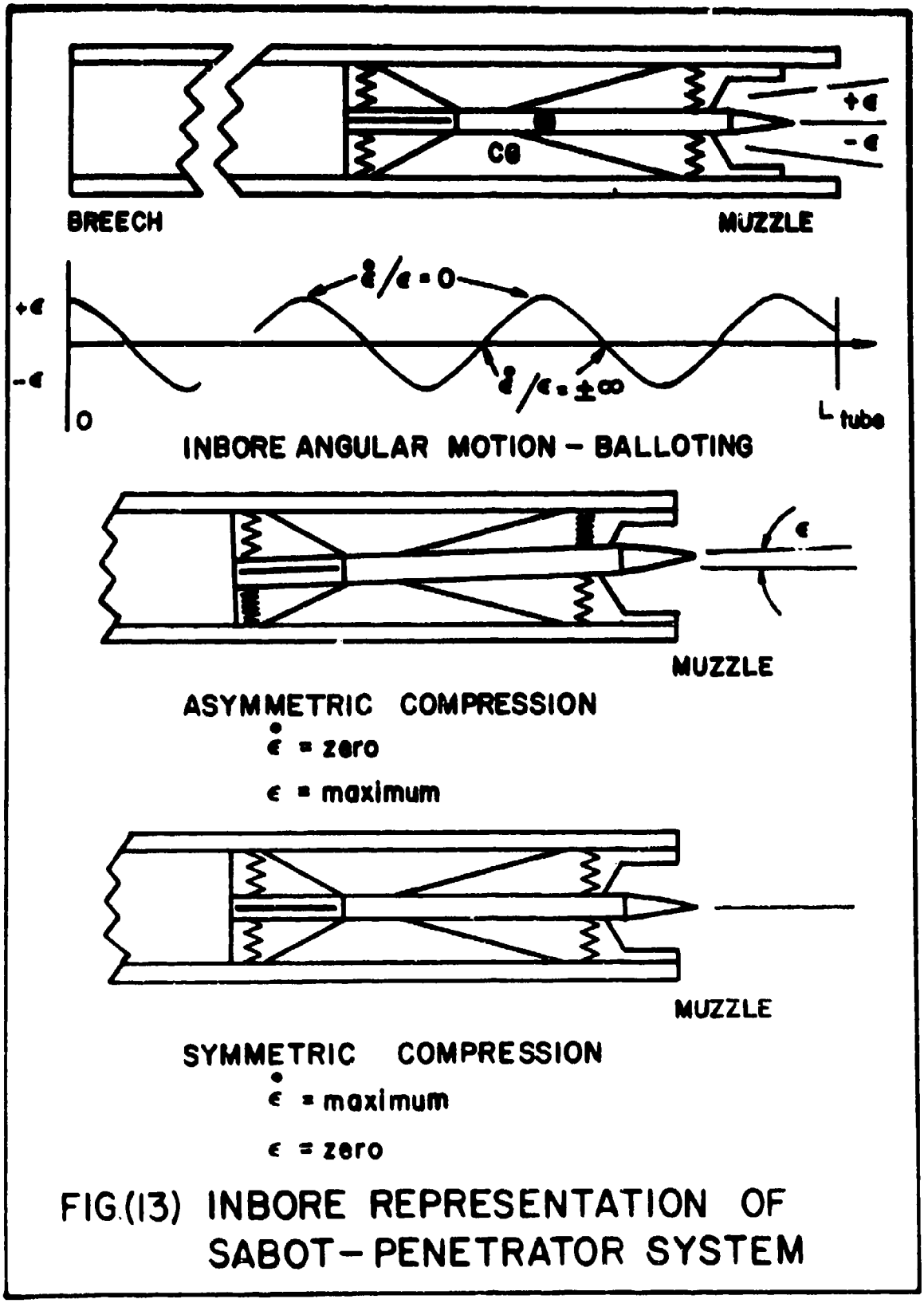

FIG.(13) INBORE REPRESENTATION OF SABOT–PENETRATOR SYSTEM

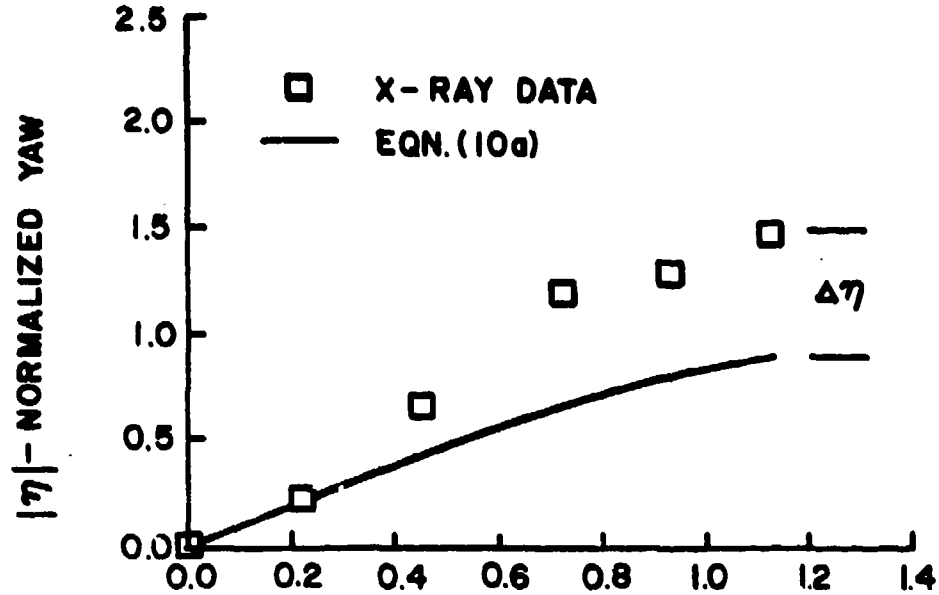

(14a) DEFINITION OF THE DISCARD DISTURBANCE – $\Delta\eta$

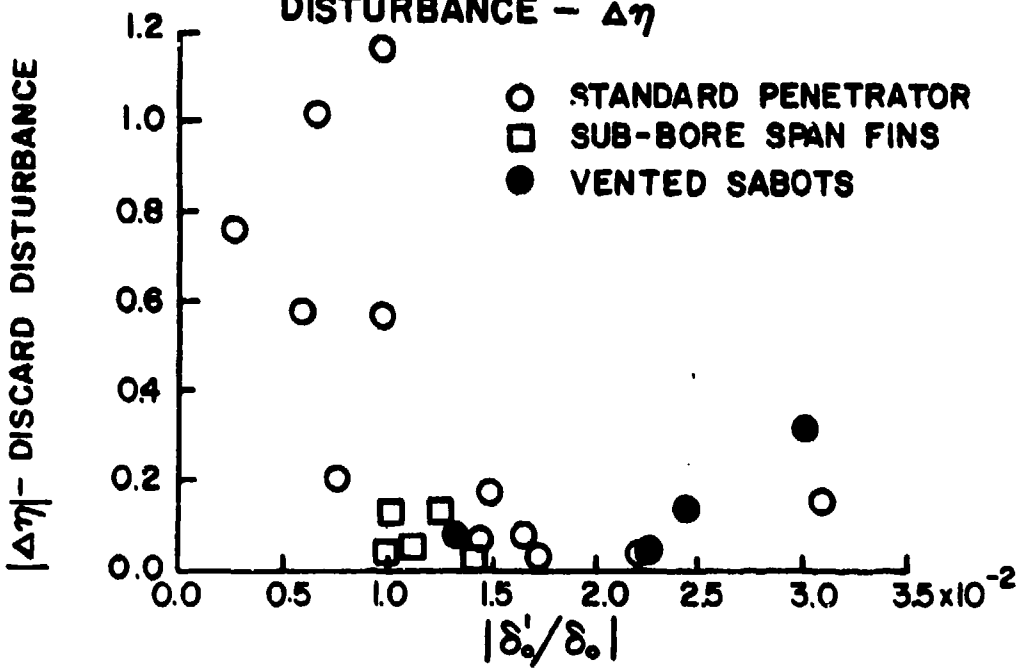

(14b) DISCARD DISTURBANCE VS. INITIAL ANGULAR RATE TO ANGLE RATIO

FIG.(14) CORRELATION OF THE DISCARD DISTURBANCE TO THE INITIAL CONDITIONS

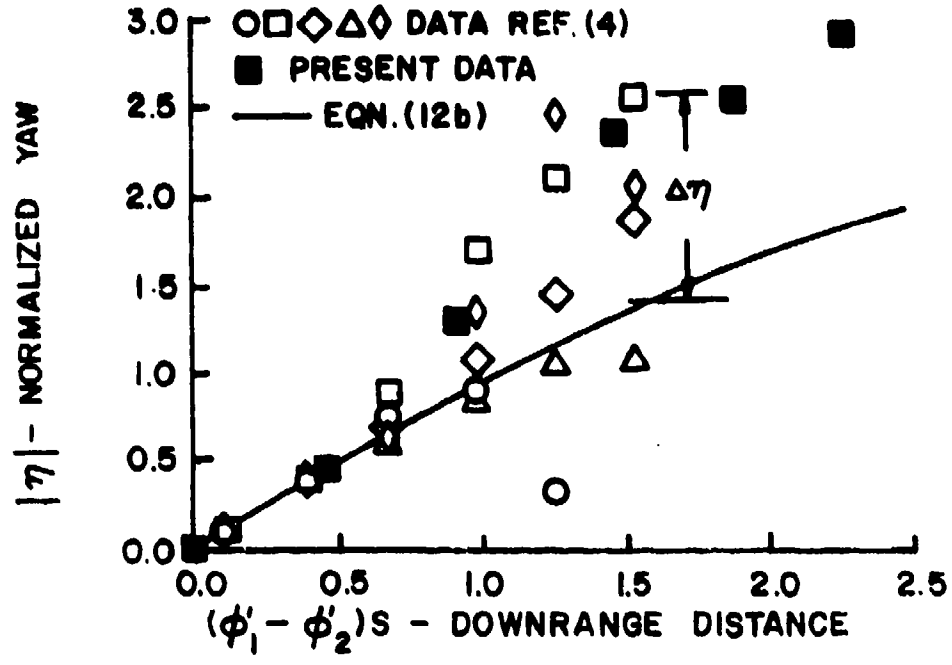

FIG.(15) COMPARISON OF THE PRESENT DATA TO PREVIOUS DATA

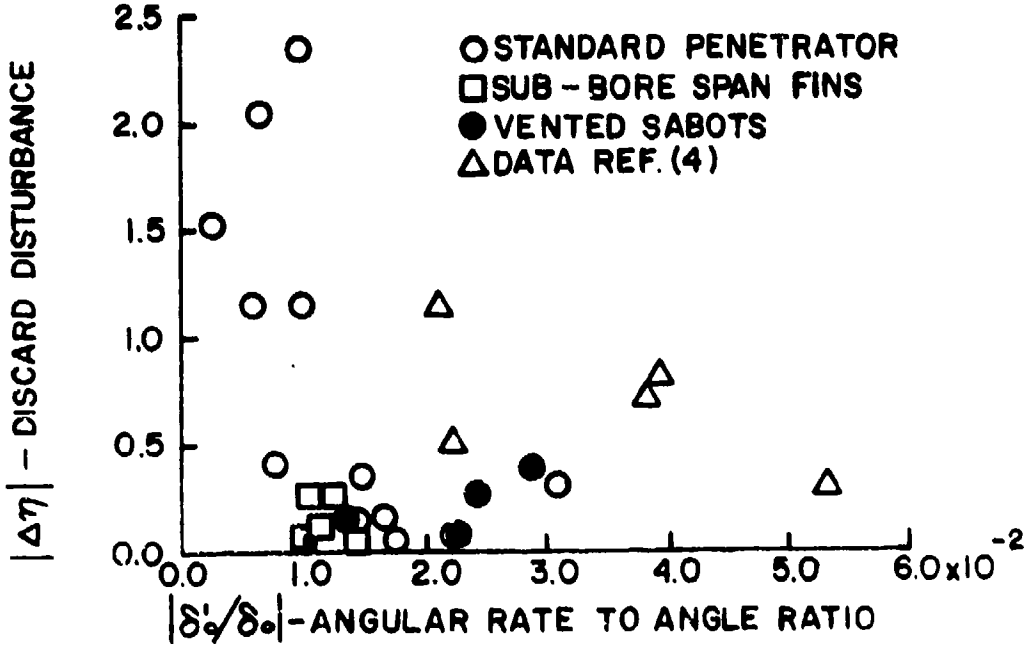

FIG.(16) COMPARISON OF THE DISCARD DISTURBANCE CORRELATIONS

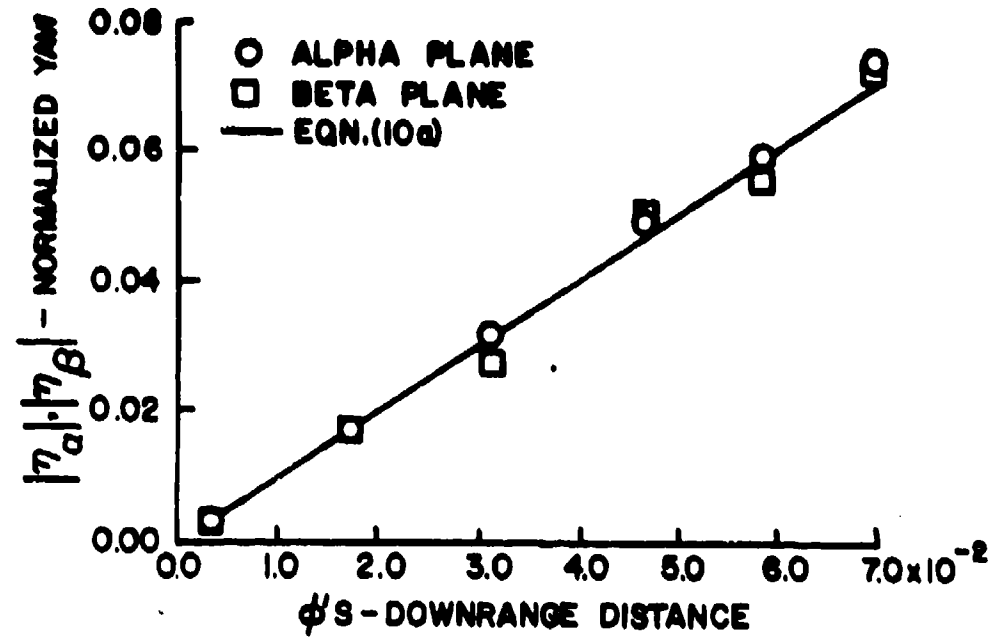

(17a) PROOF SLUG

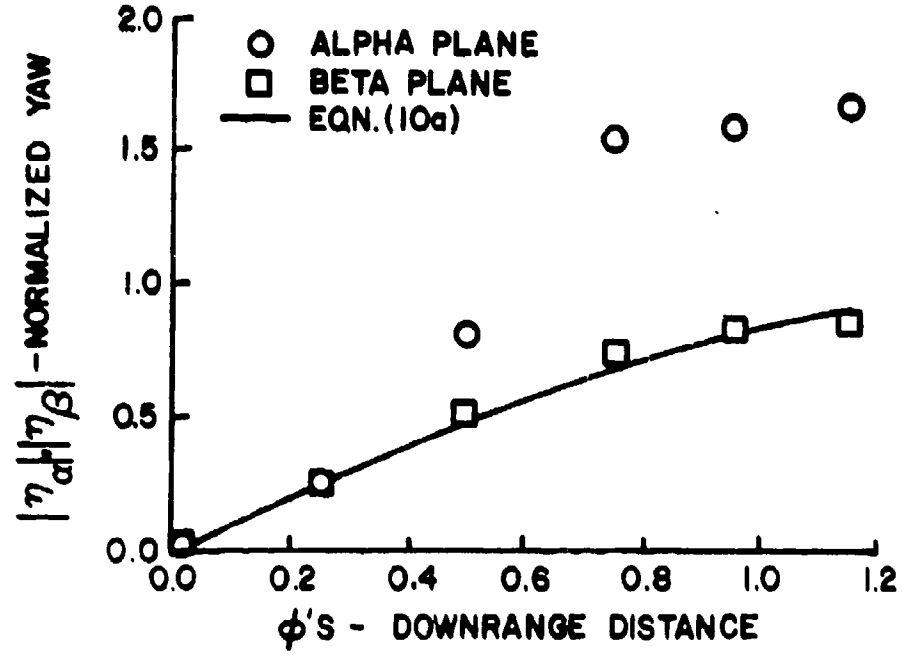

(17b) STANDARD PENETRATOR

FIG.(17) DISCARD DISTURBANCES IN THE ALPHA AND BETA PLANES

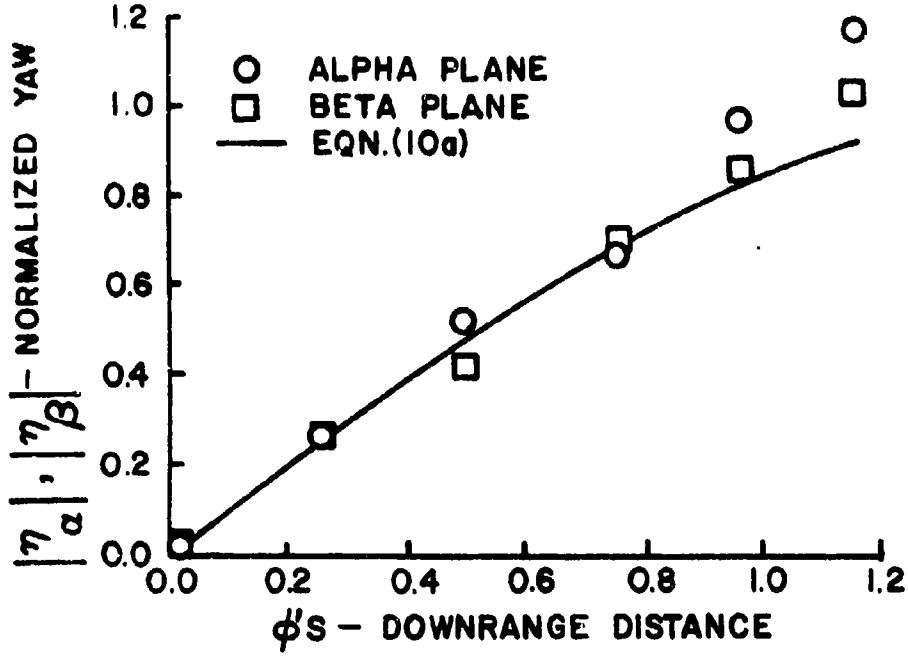

(17c) PENETRATOR-VENTED SABOT PACKAGE

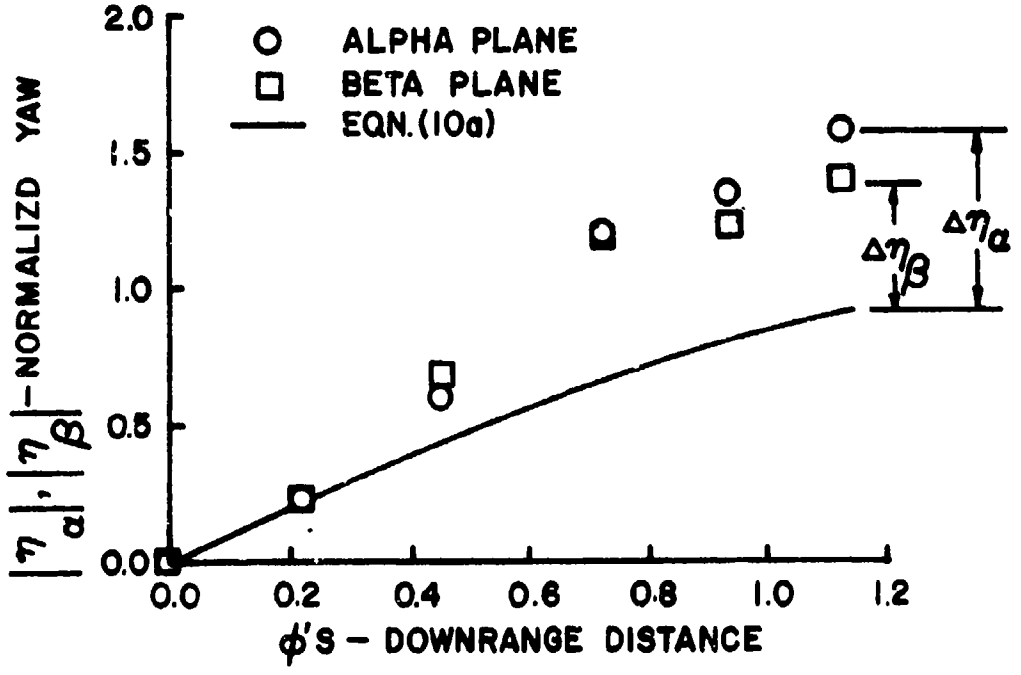

(17d) STANDARD PENETRATOR

FIG.(17) CONTINUED

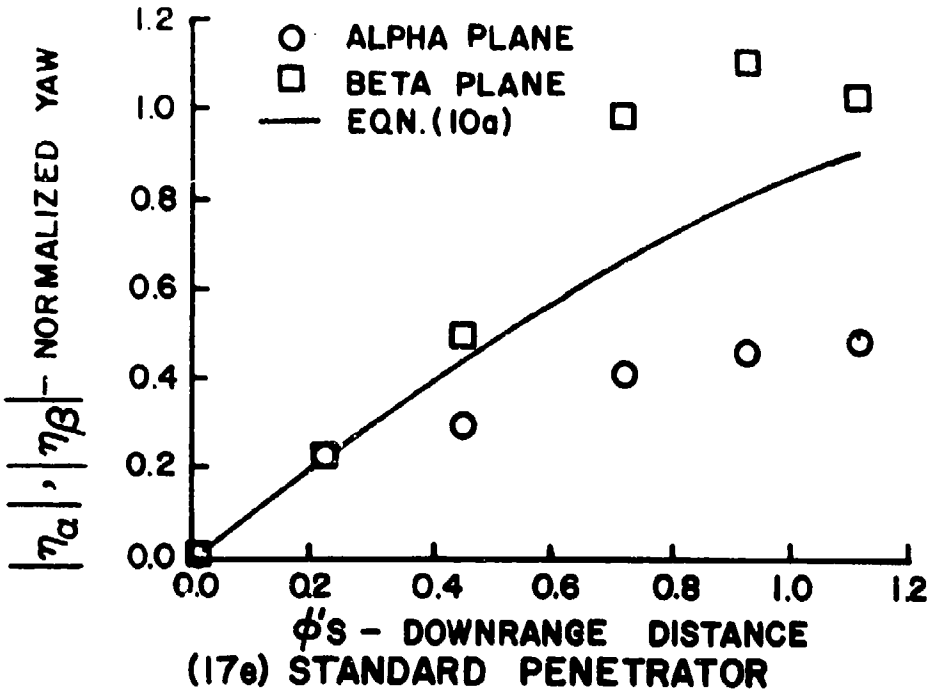

(17e) STANDARD PENETRATOR

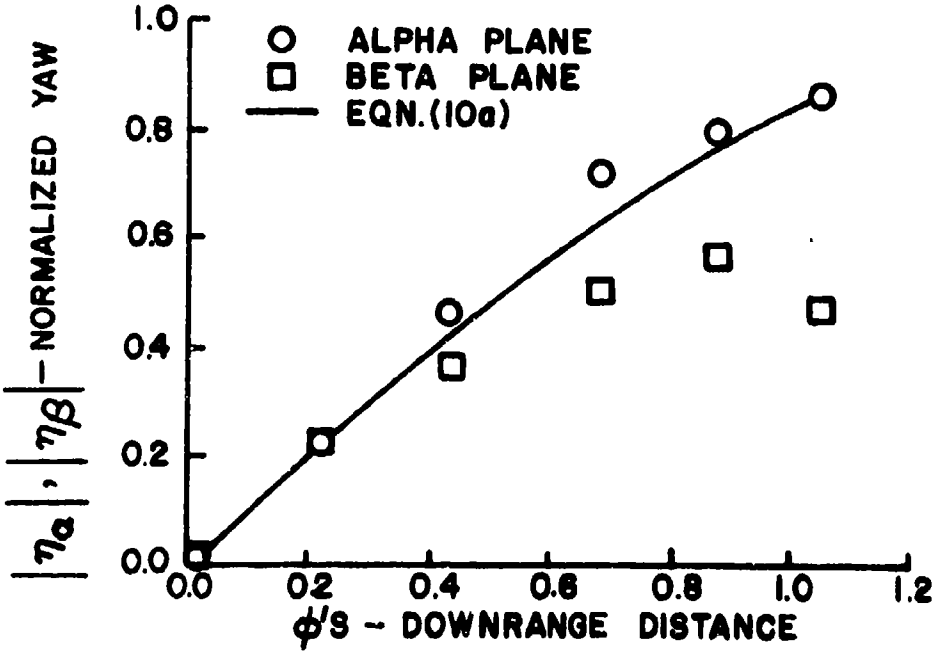

(17f) PENETRATOR WITH SUB-BORE SPAN FINS

FIG.(17) CONTINUED

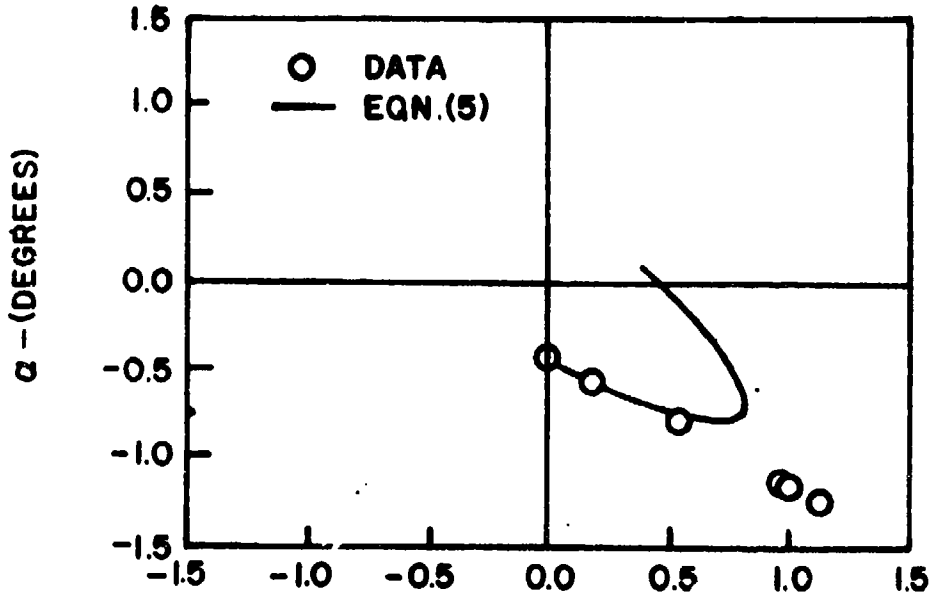

(18a) STANDARD PENETRATOR

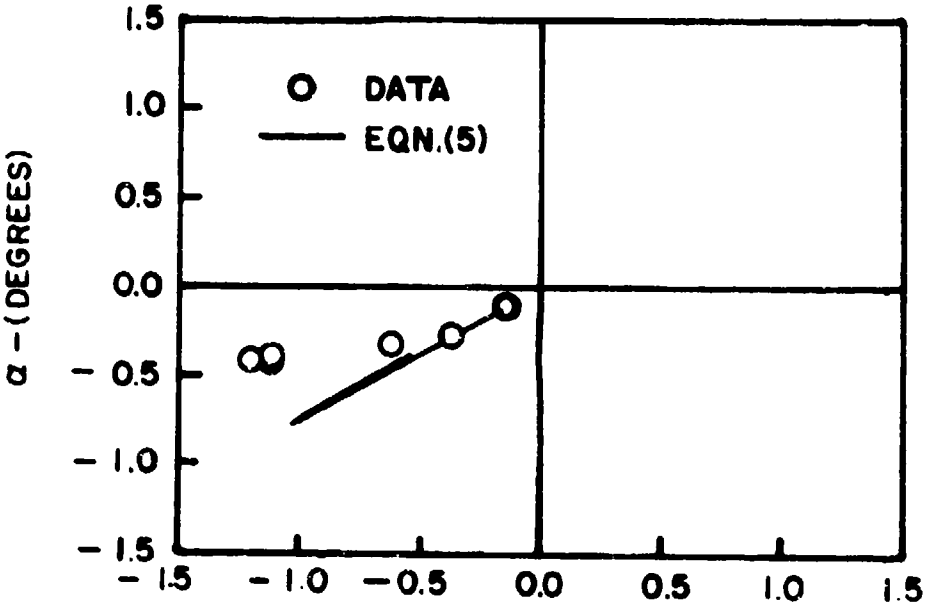

(18b) STANDARD PENETRATOR

FIG.(18) ANGLE OF ATTACK VS. ANGLE OF SIDESLIP

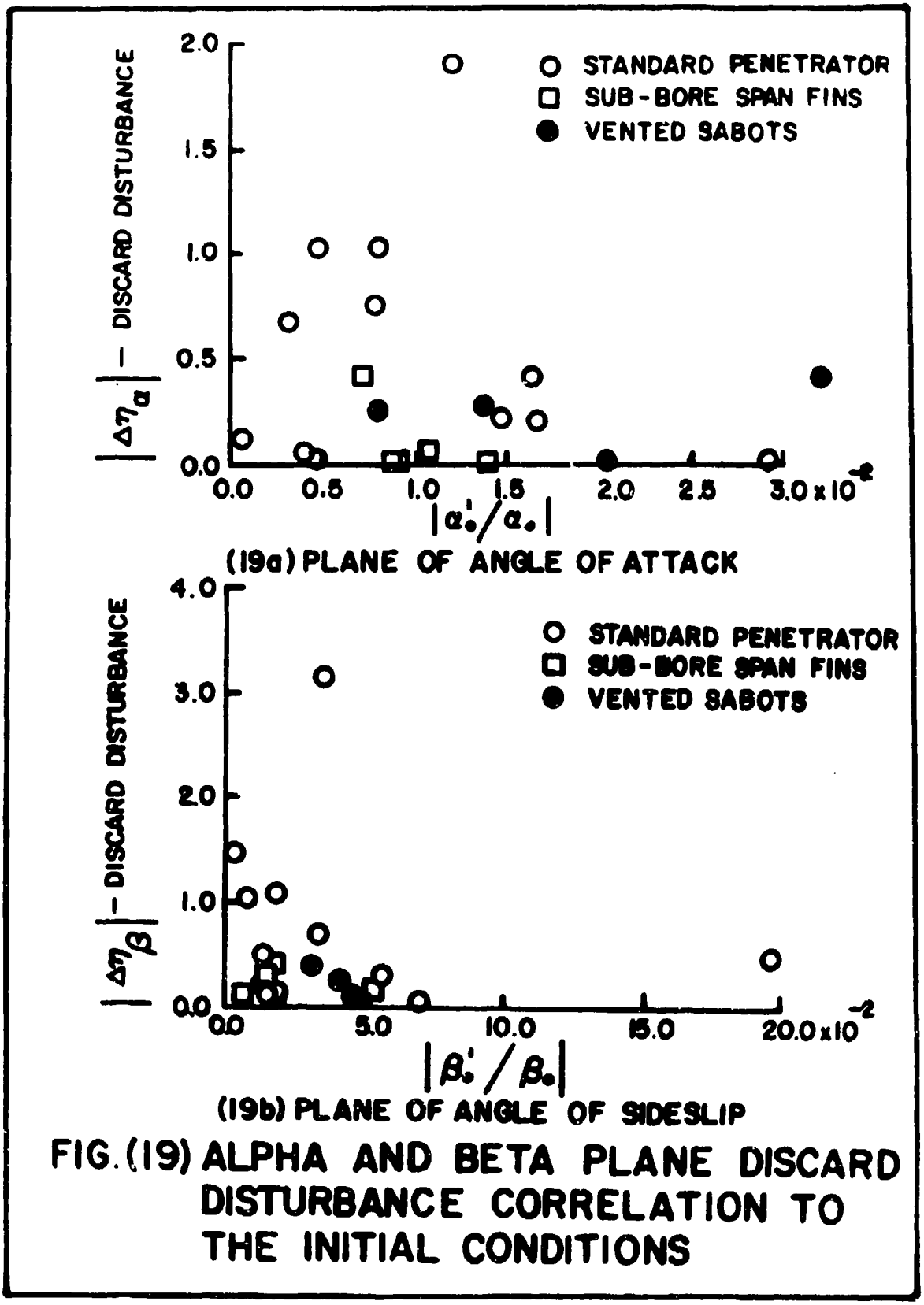

FIG. (19) ALPHA AND BETA PLANE DISCARD DISTURBANCE CORRELATION TO THE INITIAL CONDITIONS

ACKNOWLEDGMENTS

Many people contributed to the successful completion of this report and I wish to thank them in total first and then mention a few specifically. It was a learning experience to work with Mr. Donald McClellan, Mr. William Thompson, the Aerodynamic Range crew and the Transonic Range crew during the actual test program. Recognition for their efforts in data reduction to Messrs. Steve Duffy, James Carduff and the erudite Mr. James Bradley. Special thanks to Dr. E. M. Schmidt, Mr. Robert McCoy, Mr. Fred Brandon, and Mr. William Mermagen for interesting and fruitful discussions on the project.

REFERENCES

1. W. H. Drysdale, "Design of Kinetic Energy Projectiles for Structural Integrity," U. S. Army Ballistic Research Laboratory, Aberdeen Proving Ground, Maryland, BRL Report ARBRL-TR-02365, September 1981 (AD A105502).

2. C. H. Murphy, "Free Flight Motion of Symmetric Missiles," U. S. Army Ballistic Research Laboratory, Aberdeen Proving Ground, Maryland, BRL Technical Report 1216, July 1963 (AD 442757).

3. E. M. Schmidt, "Disturbance to the Launch of Fin-Stabilized Projectiles," Journal of Spacecraft and Rockets, Vol. 19, No. 1, January-February 1982, p. 30.

4. E. M. Schmidt and D. D. Shear, "Aerodynamic Interference During Sabot Discard," U. S. Army Ballistic Research Laboratory, Aberdeen Proving Ground, Maryland, BRL Report 2019, September 1977, (AD 050308). Also Journal of Spacecraft and Rockets, Vol. 15, No. 3, May-June 1978, pp. 162-167.

5. E. M. Schmidt and D. D. Shear, "Launch Dynamics of a Single Flechette Round," U. S. Army Ballistic Research Laboratory, Aberdeen Proving Ground, Maryland, BRL Report 1810, August 1975 (AD B006781).

6. W. D. Glauz, "Estimation of the Forces on a Single Flechette Resulting from a Shock Wave," Midwest Research Institute, Kansas City, Missouri, Final Report 19 June 1970 - 18 March 1971, May 1971 (AD 724178).

7. G. Glotz, "Investigation of the Stability of the Flow During the Sabot Discard Process," Sixth International Symposium on Ballistics, Orlando, Florida, 27-29 October 1981.

8. P. Crimi and D. Siegelman, "Analysis of Mechanical and Gasdynamic Loadings During Sabot Discard from Gun-Launched Projectiles," U. S. Army Ballistic Research Laboratory, Aberdeen Proving Ground, Maryland, BRL Contract Report 341, June 1977 (AD B020019).

9. E. M. Schmidt, "Wind Tunnel Measurements of Sabot Discard Aerodynamics," U. S. Army Ballistic Research Laboratory, Aberdeen Proving Ground, Maryland, BRL Technical Report ARBRL-TR-02246, July 1980 (AD 088900).

10. E. M. Schmidt and P. Plostins, "Aerodynamics of Asymmetric Sabot Discard," U. S. Army Ballistic Research Laboratory, Aberdeen Proving Ground, Maryland, BRL Report ARBRL-MR-03281, June 1983 (AD 130011).

11. E. M. Schmidt, B. P. Burns, and G. Samos, "Replica Modeling of the Launch and Flight Dynamics of Projectiles," U. S. Army Ballistic Research Laboratory, Aberdeen Proving Ground, Maryland, BRL Technical Report ARBRL-TR-02104, September 1978 (AD A063521).

12. J. N. Walbert, "Analysis of the In Bore Motion of Several Types of Projectiles," U. S. Army Ballistic Research Laboratory, Aberdeen Proving Ground, Maryland, BRL Memorandum Report ARBRL-MR-03293, July 1983 (AD B076398L).

13. W. F. Braun, "Fiducial Systems for Free Flight Spark Ranges," U. S. Army Ballistic Research Laboratory, Aberdeen Proving Ground, Maryland, BRL Memorandum Report BRLMR 2009, September 1969 (AD 860693).

14. C. H. Murphy, "Data Reduction for Free Flight Spark Ranges," U. S. Army Ballistic Research Laboratory, Aberdeen Proving Ground, Maryland, BRL Report BRLR 900, February 1954 (AD 35833).

15. P. Crimi and D. Siegleman, "Projectile/Sabot Discard Aerodynamics," U. S. Army Ballistic Research Laboratory, Aberdeen Proving Ground, Maryland, BRL Contract Report ARBRL-CR-410, December 1979 (AD 080538).

16. D. Siegelman and J. Wang, "Sabot Design Optimization," U. S. Army Ballistic Research Laboratory, Aberdeen Proving Ground, Maryland, BRL Contract Report ARBRL-CR-450, March 1981 (AD 100264).

17. D. Siegelman, J. Wang, and P. Crimi, "Computation of Sabot Discard,"U.S Army Ballistic Research Laboratory, Aberdeen Proving Ground, Maryland BRL Contract Report ARBRL-CR-505, February 1983 (AD B0715192).

LIST OF SYMBOLS

A	penetrator frontal area
C_D	penetrator drag coefficient
$C\ell_\alpha$	lift curve slope
Cm_α	static moment coefficient
d	penetrator diameter
Ia	aerodynamic angular discard impulse
Im	mechanical angular discard impulse
I_x	penetrator roll moment of inertia
I_y	penetrator transverse moment of inertia
M	defined in equation (13b)
p	penetrator roll rate
P	defined in equation (13c)
S	downrange distance (calibers)
t	time (sec)
V	penetrator velocity

GREEK SYMBOLS

α	angle of attack
β	angle of sideslip
δ	magnitude of yaw
ϵ	balloting angle
η	normalized yaw
η_α	normalized yaw alpha plane
η_β	normalized yaw beta plane
$\tilde{\xi}$	complex yaw $\tilde{\xi} = (\tilde{\beta} + i\tilde{\alpha})$

LIST OF SYBMOLS (continued)

ρ	air density
ϕ'	yaw frequency (rad/cal)
ϕ_0	initial balloting angle (Equation 11a)
ω	balloting frequency

SUPERSCRIPTS

$'$	differentiation with respect to S
o	differentiation with respect to t
~	signifying non-rolling coordinate system for ξ (see Reference 2)

SUBSCRIPTS

o	initial value at the muzzle of the gun

DISTRIBUTION LIST

No. of Copies	Organization
12	Administrator Defense Technical Info Center ATTN: DTIC-DDA Cameron Station Alexandria, VA 22314
1	Commander US Army Materiel Development and Readiness Command ATTN: DRCDRA-ST 5001 Eisenhower Avenue Alexandria, VA 22333
1	Commander US Army Materiel Development and Readiness Command ATTN: DRCDL 5001 Eisenhower Avenue Alexandria, VA 22333
4	Commander US Army Aviation Research and Development Command ATTN: Tech Dir (Mr. R. Lewis) DRDAV-E DRCPM-AAH (Mr. Corgiatt) Product Manager, AH-1 4300 Goodfellow Boulevard St. Louis, MO 63120
1	Director US Army Air Mobility Research and Development Laboratory Ames Research Center Moffett Field, CA 94035
1	Commander US Army Electronics Research and Development Command Technical Support Activity ATTN: DELSD-L Fort Monmouth, NJ 07703
1	Commander US Army Materiel Development and Readiness Command ATTN: DRCDE-R, Mr. Lockert 5001 Eisenhower Avenue Alexandria, VA 22333
1	President US Army Aviation Board ATTN: ATZQ-OP-AA Ft. Rucker, AL 36360
1	Commander US Army Medical Research and Development Command ATTN: SGRD-ZBM-C/LTC Lamothe Ft. Detrick, MD 21701
1	Commander US Army Communications Rsch and Development Command ATTN: DRSEL-ATDD Fort Monmouth, NJ 07703
1	Commander US Army Missile Command ATTN: DRSMI-R Redstone Arsenal, AL 35898
1	Commander US Army Missile Command ATTN: DRSMI-RBL Redstone Arsenal, AL 35898
1	Commander US Army Missile Command ATTN: DRSMI-TLH Redstone Arsenal, AL 35898
1	Commander US Army Missile Command ATTN: DRSMI-RDK Redstone Arsenal, AL 35898
1	Commander US Army Missile Command ATTN: DRSMI-YDL Redstone Arsenal, AL 35898
1	Commander US Army Tank Automotive Research & Development Cmd ATTN: DRSTA-TSL Warren, MI 48090

DISTRIBUTION LIST (Continued)

No. of Copies	Organization
1	Commander US Army Armament Munitions & Chemical Command ATTN: DRSMC-LEP-L(R) Rock Island, IL 61299
7	Commander US Army Armament, Munitions & Chemical Command, ARDC ATTN: DRSMC-TSS(D) DRSMC-TDS(D), Mr. Lindner DRSMC-LC-F(D), Mr. Loeb DRSMC-LCW(D), Mr. M. Salsbury DRSMC-LCW(D), Mr. R. Wrenn DACPM-CAWS(D), Mr. Barth DRSMC-SEM(D), W. Bielauskas Dover, NJ 07801
1	ODCSI, USAREUR & 7A ATTN: AEAGB-PD-PM(S&E) APO, NY 09403
1	Director Division of Medicine WRAIR/WRAMC ATTN: SGRD-UWH-D/MAJ Jaeger Washington, DC 20012
6	Commander Armament R&D Center US Army AMCCOM ATTN: DRSMC-LCV(D), Mr. Reisman DRSMC-SCA(D), Mr. Kahn DRSMC-LC(D), Dr. Frasier DRSMC-SCW(D), Mr. Townsend DRSMC-TDC(D) DRSMC-SG(D), Dr. T. Hung Dover, NJ 07801
4	Director Benet Weapons Laboratory Armament R&D Center US Army AMCCOM ATTN: DRSMC-LCB-TL(D) CPT R. Dillon Dr. G. Carofano Dr. C. Andrade Watervliet, NY 12189

No. of Copies	Organization
1	Commander US Army Jefferson Proving Ground Madison, IN 47250
1	Commander US Army Materials and Mechanics Research Center ATTN: DRXMR-ATL Watertown, MA 02172
1	Commander US Army Natick Research and Development Laboratories ATTN: DRDNA-DT Dr. D. Sieling Natick, MA 01762
1	Commander US Army Aeromedical Research Laboratory ATTN: SGRD-UAH-AS, Dr. Patterson P.O. Box 577 Ft. Rucker, AL 36360
1	Director US Army TRADOC Systems Analysis Activity ATTN: ATAA-SL White Sands Missile Range NM 88002
1	Commandant US Army Infantry School ATTN: ATSH-CD-CSO-OR Ft. Benning, GA 31905
1	Commander US Army Research Office ATTN: CRD-AA-EH P.O. Box 1211 Research Triangle Park NC 27709
1	Commander US Army Ballistic Missile Defense Systems Command Huntsville, AL 35807
1	HQDA (DAMA-ART-M) Washington, DC 20310

DISTRIBUTION LIST (Continued)

No. of Copies	Organization
3	Commander Naval Air Systems Command ATTN: AIR-604 Washington, DC 20360
3	Commander Naval Sea Systems Command ATTN: SEA-62R2 Washington, DC 20360
2	Commander and Director David W. Taylor Naval Ship Research & Development Ctr ATTN: Lib Div, Code 522 Aerodynamic Lab Bethesda, MD 20084
3	Commander Naval Surface Weapons Center ATTN: 6X, Mr. F. H. Maille Dr. J. Yagla Dr. G. Moore Dahlgren, VA 22448
1	Commander Naval Surface Weapons Center ATTN: Code 730, Tech Lib Silver Spring, MD 20910
1	Commander Naval Weapons Center ATTN: Code 3431,Tech Lib China Lake, CA 93555
1	Commander Naval Weapons Center ATTN: Tech Info Div Washington, DC 20375
1	Commander Naval Ordnance Station ATTN: Code FS13A, P. Sewell Indian Head, MD 20640
1	Commander US Army Development & Employment Agency ATTN: MODE-TED-SAB Fort Lewis, WA 98433

No. of Copies	Organization
2	AFATL (DLDL, Dr. D. Daniels) Tech Lib) Eglin AFB, FL 32542
1	AFWL/SUL Kirtland AFB, NM 87117
1	ASD/XRA (STINFO) Wright-Patterson AFB, OH 45433
1	Director National Aeronautics and Space Administration George C. Marshall Space Flight Center ATTN: MS-I, Lib Huntsville, AL 38512
1	Director Jet Propulsion Laboratory ATTN: Tech Lib 2800 Oak Grove Drive Pasadena, CA 91109
1	Director NASA Scientific & Technical Information Facility ATTN: SAK/DL P.O. Box 8757 Baltimore/Washington International Airport, MD 21240
1	AAI Corporation ATTN: Dr. T. Stastny Cockeysville, MD 21030
1	Advanced Technology Labs ATTN: Mr. J. Erdos Merrick & Steward Avenues Westbury, NY 11590
1	Aerospace Corporation ATTN: Dr. G. Widhopf P.O. Box 92957 Los Angeles, CA 90009

DISTRIBUTION LIST (Continued)

No. of Copies	Organization
1	ARTEC Associates, Inc. ATTN: Dr. S. Gill 26046 Eden Landing Road Hayward, CA 94545
1	AVCO Systems Division ATTN: Dr. D. Siegelman 201 Lowell Street Wilmington, MA 01887
1	Battelle Columbus Laboratories ATTN. Donald J. Butz 505 King Avenue Columbus, OH 43201
1	Technical Director Colt Firearms Corporation 150 Huyshope Avenue Hartford, CT 14061
1	ARO, Inc Von Karman Gasdynamics Facility ATTN: Dr. J. Lewis Arnold AFS, TN 37389
1	General Electric Corporation Armaments Division ATTN: Mr. R. Whyte Lakeside Avenue Burlington, VT 05401
1	Honeywell, Inc. ATTN: Mail Station MN 112190 (G. Stilley) 600 Second Street, North Hopkins, MN 55343
1	Hughes Helicopter Company Bldg. 2, MST22B ATTN: Mr. R. Forker Centinella and Teel Streets Culver City, CA 90230
1	Martin Marietta Aerospace ATTN: Mr. A. J. Culotta P.O. Box 5387 Orlando, FL 32805

No. of Copies	Organization
1	Olin Corporation Winchester Western Division New Haven, CT 06504
1	Sandia National Laboratory ATTN: Aerodynamics Dept Org 5620, R. Maydew Albuquerque, NM 87115
1	Guggenheim Aeronautical Lab California Institute of Tech ATTN: Tech Lib Pasadena, CA 91104
1	Franklin Institute ATTN: Tech Lib Race & 20th Streets Philadelphia, PA 19103
1	Director Applied Physics Laboratory The Johns Hopkins University John Hopkins Road Laurel, MD 20707
1	Massachusetts Institute of Technology Dept of Aeronautics and Astronautics ATTN: Tech Lib 77 Massachusetts Avenue Cambridge, MA 02139
1	Ohio State University Dept of Aeronautics and Astronautical Engineering ATTN: Tech Lib Columbus, OH 43210
3	Polytechnic Institute of New York Graduate Center ATTN: Tech Lib Prof. S. Lederman Prof. R. Cresci Route 110 Farmingdale, NY 11735

DISTRIBUTION LIST (Continued)

No. of Copies — Organization

1 Director
Forrestal Research Center
Princeton University
Princeton, NJ 08540

1 Kaman Tempo
ATTN: Mr. J. Hindes
816 State Street
P.O. Drawer QQ
Santa, Barbara, CA 93102

1 Southwest Research Institute
ATTN: Mr. Peter S. Westine
8500 Culebra Road
San Antonio, TX 78228

2 Boeing Aerospace Corporation
ATTN: C. R. Pond
P. D. Texeira
MS 8C-64
PO Box 3999
Seattle, Washington 98124

Aberdeen Proving Ground

Dir, USAMSAA
ATTN: DRXSY-D
DRXSY-MP, H. Cohen

Cdr, USATECOM
ATTN: DRSTE-TO-F

Cdr, CRDC, AMCCOM
ATTN: DRSMC-CLB-PA
DRSMC-CLN
DRSMC-CLJ-L

Dir, USAHEL
ATTN: Dr. Weisz
Dr. Cummings
Mr. Garinther

Cdr, USATECOM
ATTN: MTD, Mr. S.Walton

USER EVALUATION SHEET/CHANGE OF ADDRESS

This Laboratory undertakes a continuing effort to improve the quality of the reports it publishes. Your comments/answers to the items/questions below will aid us in our efforts.

1. BRL Report Number_____ Date of Report_____

2. Date Report Received_____

3. Does this report satisfy a need? (Comment on purpose, related project, or other area of interest for which the report will be used.)_____

4. How specifically, is the report being used? (Information source, design data, procedure, source of ideas, etc.)_____

5. Has the information in this report led to any quantitative savings as far as man-hours or dollars saved, operating costs avoided or efficiencies achieved, etc? If so, please elaborate._____

6. General Comments. What do you think should be changed to improve future reports? (Indicate changes to organization, technical content, format, etc.)

CURRENT ADDRESS

Name

Organization

Address

City, State, Zip

7. If indicating a Change of Address or Address Correction, please provide the New or Correct Address in Block 6 above and the Old or Incorrect address below.

OLD ADDRESS

Name

Organization

Address

City, State, Zip

(Remove this sheet along the perforation, fold as indicated, staple or tape closed, and mail.)